

Dynamical System Identification, Model Selection and Model Uncertainty Quantification by Bayesian Inference

Robert K. Niven,^{1, a)} Laurent Cordier,² Ali Mohammad-Djafari,³ Markus Abel,⁴ and
Markus Quade⁴

¹⁾*School of Engineering and Technology, The University of New South Wales,
Canberra, ACT, 2600, Australia*

²⁾*Institut Pprime, CNRS – Université de Poitiers – ISAE-ENSMA, UPR 3346,
France*

³⁾*Laboratoire des signaux et systèmes (L2S), CentraleSupélec, Gif-sur-Yvette,
France*

⁴⁾*Ambrosys GmbH, Potsdam, Germany*

(Dated: 31 January 2024)

This study presents a Bayesian maximum *a posteriori* (MAP) framework for dynamical system identification from time-series data. This is shown to be equivalent to a generalized zeroth-order Tikhonov regularization, providing a rational justification for the choice of the residual and regularization terms, respectively, from the negative logarithms of the likelihood and prior distributions. In addition to the estimation of model coefficients, the Bayesian interpretation gives access to the full apparatus for Bayesian inference, including the ranking of models, the quantification of model uncertainties and the estimation of unknown (nuisance) hyperparameters. Two Bayesian algorithms, joint maximum *a posteriori* (JMAP) and variational Bayesian approximation (VBA), are compared to the popular SINDy algorithm for thresholded least-squares regression, by application to several dynamical systems with added noise. For multivariate Gaussian likelihood and prior distributions, the Bayesian formulation gives Gaussian posterior and evidence distributions, in which the numerator terms can be expressed in terms of the Mahalanobis distance or “Gaussian norm” $\|\mathbf{y} - \hat{\mathbf{y}}\|_{M^{-1}}^2 = (\mathbf{y} - \hat{\mathbf{y}})^\top M^{-1}(\mathbf{y} - \hat{\mathbf{y}})$, where \mathbf{y} is a vector variable, $\hat{\mathbf{y}}$ is its estimator and M is the covariance matrix. The posterior Gaussian norm is shown to provide a robust metric for quantitative model selection.

^{a)}Electronic mail: r.niven@unsw.edu.au

A large number of natural and human phenomena are controlled by dynamical systems, commonly expressed in the form of differential or difference equations for the evolution of state variables in time. Examples include conservation laws for the flow of fluids, chemical species, momentum and energy; the laws of mechanics for harmonic oscillators, machines and planetary motion; biological population models for species growth, competition and predator-prey relations; financial demand-supply models for prices, incomes and economic growth; and combat models in military operations research. One of the great challenges of inference is to identify a dynamical system from its discrete time-series data, including its governing differential equation system and parameter values. While many methods have been used, few researchers have applied Bayesian inference, the fundamental method for the discovery of models from data. This study provides a Bayesian perspective on dynamical system identification, and illustrates several advantages over existing regularization methods.

I. INTRODUCTION

Many physical phenomena can be described by a continuous dynamical system, commonly represented by:

$$\dot{\mathbf{x}}(t) = \mathbf{f}(\mathbf{x}(t)), \quad (1)$$

where $\mathbf{x} \in \mathbb{R}^n$ is the observable state vector, generally a function of time t (and/or some other parameters), $\dot{\mathbf{x}} \in \mathbb{R}^n$ is its time derivative and \mathbf{f} is the system function or model, in general a nonlinear function of \mathbf{x} . Given a sample of discrete time-series data $[\mathbf{x}(t_1), \mathbf{x}(t_2), \mathbf{x}(t_3), \dots]$, how should we identify the model \mathbf{f} ? In its most general form, this can be described as *system identification*, while for \mathbf{f} selected from a known class of functions, the problem reduces to one of *parameter identification*. These functions may be chosen from a set of basis functions applicable to the system, or constructed from an alphabet of the data variables.

In recent years, there has been considerable interest in the use of sparse regularization methods for dynamical system identification¹⁻¹¹. These are used to infer a matrix of coefficients which can reproduce the dynamical system very precisely. Such methods usually incorporate a sparsification component to reduce the number of coefficients, such as a reg-

ularization term in the objective function. However, both the regularization term and its multiplying parameter (penalization coefficient) tend to be chosen in a heuristic or *ad hoc* manner, without much theoretical insight.

It must be noted that the fundamental method for the solution of inverse problems such as (1) is *Bayesian inference*. This involves the application of Bayes’ rule to calculate the “probability of an hypothesis or model, given the data”, or in other words, the degree of belief in the hypothesis or model, given what is known^{12–15}. The Bayesian interpretation of probabilities as “degrees of belief” or “plausibilities” has been shown to be universal and mathematically rigorous^{14,16,17}, overcoming the late-19th century restriction of probabilities to measurable frequencies^{18–21}. Bayesian inference provides a common platform for the analysis of all uncertainties, including inverse model identification, model ranking, hypothesis testing, estimation, interpolation, extrapolation, classification, experimental design or any other analysis of data, and can be used in subsequent decision frameworks such as utility / loss analysis and risk assessment.

The aim of this study is to present a Bayesian framework for dynamical system identification from time-series data, based on the Bayesian maximum *a posteriori* (MAP) estimate. This was originally developed for other purposes such as image analysis^{22–26}, but there have been some applications to dynamical systems^{27–33}. The method bears specific similarities to Bayesian dynamical system reconstruction by Gaussian processes^{34–37}, posterior exploratory methods^{38,39} or constrained computational methods⁴⁰. In §II A we first examine the formulation of regularization methods, followed in §II B by a Bayesian reinterpretation. For Gaussian multivariate prior and likelihood distributions, the MAP estimate is shown to be equivalent to a generalized zeroth-order Tikhonov regularization. This provides a rational justification for the choices of the residual and regularization terms, respectively, as the negative logarithms of the likelihood and prior distributions. We then explore further features of the Bayesian inverse method, including the Bayesian posterior and model uncertainty quantification (§II C), the posterior Bayes factor and Bayesian model selection (§II D), the Bayesian evidence (§II E), and two Bayesian algorithms for the estimation of unknown hyperparameters: joint maximum *a posteriori* (JMAP) and variational Bayesian approximation (VBA) (§II F). In §III, we then apply JMAP and VBA to the analysis of three dynamical systems with added noise, in comparison to the well-known SINDy algorithm for thresholded least-squares regression^{1,4–11}. The findings are summarized in the conclusions in §IV.

II. THEORETICAL FOUNDATIONS

A. Sparse Regression (Regularization) Methods

The application of sparse regression for dynamical system identification^{1–4} generally proceeds by the following steps. First, a set of time-series data, consisting of m time steps of an n -dimensional variable $\mathbf{x}(t)$ with elements $x_j(t_i)$, and of its derivative $\dot{\mathbf{x}}(t)$ with elements $\dot{x}_j(t_i)$, are assembled into the $m \times n$ matrices:

$$\mathbf{X} = \begin{bmatrix} \mathbf{x}^\top(t_1) \\ \vdots \\ \mathbf{x}^\top(t_m) \end{bmatrix} = \begin{bmatrix} x_1(t_1) & \dots & x_n(t_1) \\ \vdots & & \vdots \\ x_1(t_m) & \dots & x_n(t_m) \end{bmatrix} \quad \text{and} \quad (2)$$

$$\dot{\mathbf{X}} = \begin{bmatrix} \dot{\mathbf{x}}^\top(t_1) \\ \vdots \\ \dot{\mathbf{x}}^\top(t_m) \end{bmatrix} = \begin{bmatrix} \dot{x}_1(t_1) & \dots & \dot{x}_n(t_1) \\ \vdots & & \vdots \\ \dot{x}_1(t_m) & \dots & \dot{x}_n(t_m) \end{bmatrix}. \quad (3)$$

Second, an alphabet of c functions with index ℓ – chosen by a classification method or from theoretical insights into the problem – is applied to \mathbf{X} (and also if desired to $\dot{\mathbf{X}}$), to generate an $m \times c$ library matrix, for example:

$$\Theta(\mathbf{X}) = \begin{bmatrix} 1 & \mathbf{X} & \mathbf{X}^2 & \mathbf{X}^3 & \dots & \sin(\mathbf{X}) & \cos(\mathbf{X}) & \dots \end{bmatrix}, \quad (4)$$

here expressed in terms of functions of the columns of (2). The dynamical system (1) is thereby converted to the discrete linear map:

$$\dot{\mathbf{X}} = \Theta(\mathbf{X})\Xi, \quad (5)$$

in which Ξ is a $c \times n$ matrix of coefficients $\xi_{\ell j} \in \mathbb{R}$, representing the model \mathbf{f} . For multivariate data, eq. (5) can be resolved columnwise, i.e., by considering a succession of problems in which $\dot{\mathbf{X}}_j$ and Ξ_j correspond to the j th columns of $\dot{\mathbf{X}}$ and Ξ , respectively.

Third, (5) is solved to determine the matrix Ξ . The simplest inversion method is least squares regression, involving minimization of an objective function based on the residual sum of squares^{41,42}:

$$\begin{aligned} \hat{\Xi}_j^{\text{LS}} &= \arg \min_{\Xi_j} J^{\text{LS}}(\Xi_j), \\ J^{\text{LS}}(\Xi_j) &= \|\dot{\mathbf{X}}_j - \Theta(\mathbf{X})\Xi_j\|_2^2 \end{aligned} \quad (6)$$

where $\hat{\Xi}_j^{\text{LS}}$ is the inferred solution and $\|\mathbf{y}\|_2 = \sqrt{\mathbf{y}^\top \mathbf{y}}$ is the L_2 or Euclidean norm for the vector quantity \mathbf{y} . However, in practice (5) will contain noise, causing computational difficulties and the generation of spurious coefficients in $\hat{\Xi}_j^{\text{LS}}$. This is generally handled by a sparse regression method, in which an additional regularization term is added to the objective function^{41–45}:

$$\hat{\Xi}_j^{\text{reg}} = \arg \min_{\Xi_j} J^{\text{reg}}(\Xi_j), \quad (7)$$

$$J^{\text{reg}}(\Xi_j) = \|\dot{\mathbf{X}}_j - \Theta(\mathbf{X})\Xi_j\|_\beta^\alpha + \kappa_j \|\Xi_j\|_\delta^\gamma,$$

where in general $\|\mathbf{y}\|_p = (\sum_i |y_i|^p)^{1/p}$ is the L_p norm with $p \in \mathbb{R}$ for the vector quantity \mathbf{y} , $\kappa_j \in \mathbb{R}$ is the regularization coefficient and $\alpha, \beta, \gamma, \delta \in \mathbb{R}$ are constants. For dynamical system identification, (7) has been implemented with $\alpha, \gamma \in \{1, 2\}$, $\beta = 2$ and $\delta \in \{0, 1, 2\}$, including ridge regression^{42,44} for $\alpha, \beta, \gamma, \delta = 2$, the least absolute shrinkage and selection operator (LASSO)^{45,46} or sparse optimization² for $\alpha, \beta = 2$ and $\gamma, \delta = 1$, and strong sparsity³ for $\alpha, \beta = 2$, $\gamma = 1$ and $\delta = 0$. These methods have close connections to other classification techniques such as principal orthogonal decomposition (POD), singular value decomposition (SVD), dynamic mode decomposition (DMD) and Koopman analysis^{41,47–49}.

Alternatively, instead of (7), some authors have enforced a sparse model by iterative thresholding, termed the sparse identification of nonlinear dynamics (SINDy) method^{1,4–11}:

$$J^{\text{IT}}(\Xi_j) = \|\dot{\mathbf{X}}_j - \Theta(\mathbf{X})\Xi_j\|_2^2 \quad \text{with} \quad |\xi_{\ell j}| \geq \lambda, \forall \ell, \forall j \quad (8)$$

where λ is a threshold parameter. This has been shown⁵⁰ to converge to (7) with $\alpha = \beta = 2$ and $\gamma = 0$.

We note that in most previous applications, the regularization term in (7) and parameter κ_j – or the threshold λ in (8) – are selected by heuristic methods, to prefer solutions with smaller norms and/or based on user judgments of the numerical performance. Some authors have selected the SINDy λ based on metrics such as the Akaike information criterion (AIC), to prefer models with fewer coefficients⁴. Other methods for selection of κ_j include cross-validation and generalized cross-validation, unbiased predictive risk estimators, the discrepancy principle and the L-curve principle^{41,42}. The selection of the appropriate model class, and comparisons between individual models, are also largely based on qualitative criteria and user judgment. Some authors^{27–33} have applied Bayesian regularization methods to dynamical system identification, the subject of this study.

B. Bayesian Regularization

To construct a Bayesian solution to the above inverse problem^{22–26,41}, we first recognize that each component of the discrete linear map (5) should be written as:

$$\dot{\mathbf{X}}_j = \Theta(\mathbf{X})\Xi_j + \epsilon_j \quad (9)$$

where ϵ_j is an m -dimensional error (noise) vector, representing the uncertainty in the measurement data. The variables $\dot{\mathbf{X}}_j$, \mathbf{X} , Ξ_j and ϵ_j are considered to be probabilistic, each represented by a probability density function (pdf) defined over their domain. Instead of inverting (9), the Bayesian inversion proceeds by calculating the posterior probability density function (pdf) of Ξ_j conditioned on the observed data $\dot{\mathbf{X}}_j$, given by Bayes' rule^{12–15}:

$$p(\Xi_j|\dot{\mathbf{X}}_j) = \frac{p(\dot{\mathbf{X}}_j|\Xi_j)p(\Xi_j)}{p(\dot{\mathbf{X}}_j)} \propto p(\dot{\mathbf{X}}_j|\Xi_j)p(\Xi_j) \quad (10)$$

where $p(\Xi_j)$ is the prior pdf, $p(\dot{\mathbf{X}}_j|\Xi_j)$ is the likelihood and $p(\dot{\mathbf{X}}_j)$ is the evidence. The simplest Bayesian method is the maximum *a posteriori* (MAP) point estimate of Ξ_j , given by the maximum of (10). For higher fidelity, it is usual to calculate the logarithmic maximum, from (10) giving the estimator:

$$\hat{\Xi}_j^{\text{MAP}} \cong \arg \max_{\Xi_j} [\ln p(\dot{\mathbf{X}}_j|\Xi_j) + \ln p(\Xi_j)]. \quad (11)$$

in which the evidence $p(\dot{\mathbf{X}}_j)$ is assumed near-constant.

To compute the solution to (11), we must assign expressions to the probability distributions $p(\dot{\mathbf{X}}_j|\Xi_j)$ and $p(\Xi_j)$. First, we assume that ϵ_j consists of unbiased multivariate Gaussian noise with the $m \times m$ covariance matrix \mathbf{V}_{ϵ_j} ²⁵:

$$p(\epsilon_j|\Xi_j) = \mathcal{N}(\epsilon_j; \mathbf{0}, \mathbf{V}_{\epsilon_j}) = \frac{\exp(-\frac{1}{2}\|\epsilon_j\|_{\mathbf{V}_{\epsilon_j}^{-1}}^2)}{\sqrt{(2\pi)^m \det(\mathbf{V}_{\epsilon_j})}}, \quad (12)$$

where $\mathbf{0}$ is a zero vector, $\det(\cdot)$ is the determinant and $\|\mathbf{y}\|_A^2 := \mathbf{y}^T A \mathbf{y}$ is the Mahalanobis distance of the vector \mathbf{y} with respect to a symmetric positive semi-definite matrix A , here referred to as a ‘‘Gaussian norm’’. This gives:

$$p(\epsilon_j|\Xi_j) \propto \exp(-\frac{1}{2}\|\epsilon_j\|_{\mathbf{V}_{\epsilon_j}^{-1}}^2), \quad (13)$$

Substituting (9) gives the likelihood:

$$\begin{aligned} p(\dot{\mathbf{X}}_j | \Xi_j) &= \mathcal{N}(\dot{\mathbf{X}}_j; \Theta(\mathbf{X})\Xi_j, \mathbf{V}_{\epsilon_j}) \\ &\propto \exp\left(-\frac{1}{2} \|\dot{\mathbf{X}}_j - \Theta(\mathbf{X})\Xi_j\|_{\mathbf{V}_{\epsilon_j}^{-1}}^2\right). \end{aligned} \quad (14)$$

Second, we adopt a multivariate Gaussian prior for Ξ_j , with zero mean $\boldsymbol{\mu}_j = \mathbf{0}$ and $c \times c$ covariance matrix \mathbf{V}_{Ξ_j} :

$$\begin{aligned} p(\Xi_j) &= \mathcal{N}(\Xi_j; \boldsymbol{\mu}_j, \mathbf{V}_{\Xi_j}) = \mathcal{N}(\Xi_j; \mathbf{0}, \mathbf{V}_{\Xi_j}) \\ &= \frac{\exp\left(-\frac{1}{2} \|\Xi_j\|_{\mathbf{V}_{\Xi_j}^{-1}}^2\right)}{\sqrt{(2\pi)^c \det(\mathbf{V}_{\Xi_j})}} \propto \exp\left(-\frac{1}{2} \|\Xi_j\|_{\mathbf{V}_{\Xi_j}^{-1}}^2\right). \end{aligned} \quad (15)$$

This represents the *a priori* belief that the model coefficients $\xi_{\ell j}$ will be positive or negative, without bias, but will not approach $\pm\infty$. The Gaussian prior gives a simple distribution of this form, which will preferentially select coefficients close to zero, yet provides support over the entire parameter space $\xi_{\ell j} \in \mathbb{R}$. For constant values m and c , covariance matrices and evidence, (11) becomes^{25,41}:

$$\begin{aligned} \hat{\Xi}_j^{\text{MAP}} &\cong \arg \max_{\Xi_j} \left[\ln \exp\left(-\frac{1}{2} \|\dot{\mathbf{X}}_j - \Theta(\mathbf{X})\Xi_j\|_{\mathbf{V}_{\epsilon_j}^{-1}}^2\right) \right. \\ &\quad \left. + \ln \exp\left(-\frac{1}{2} \|\Xi_j\|_{\mathbf{V}_{\Xi_j}^{-1}}^2\right) \right] \\ &= \arg \max_{\Xi_j} -\frac{1}{2} \left[\|\dot{\mathbf{X}}_j - \Theta(\mathbf{X})\Xi_j\|_{\mathbf{V}_{\epsilon_j}^{-1}}^2 + \|\Xi_j\|_{\mathbf{V}_{\Xi_j}^{-1}}^2 \right] \\ &= \arg \min_{\Xi_j} \left[\|\dot{\mathbf{X}}_j - \Theta(\mathbf{X})\Xi_j\|_{\mathbf{V}_{\epsilon_j}^{-1}}^2 + \|\Xi_j\|_{\mathbf{V}_{\Xi_j}^{-1}}^2 \right]. \end{aligned} \quad (16)$$

A more complete formulation of (16) is examined in Appendix A. The Bayesian MAP estimator thus provides a generalized form of the objective function used in the traditional regularization method (7). Furthermore, as shown in Appendix A, for isotropic variances of the noise $\mathbf{V}_{\epsilon_j} = \sigma_{\epsilon_j}^2 \mathbf{I}_m$ and prior $\mathbf{V}_{\Xi_j} = \sigma_{\Xi_j}^2 \mathbf{I}_c$, where \mathbf{I}_s is the identity matrix of size s , (16) reduces to the Tikhonov regularization function (7) with $\alpha, \beta, \gamma, \delta = 2$ and $\kappa_j = \sigma_{\epsilon_j}^2 / \sigma_{\Xi_j}^2$.

We see from (16) that regularization by the Bayesian MAP method, assuming Gaussian prior and likelihood functions, is equivalent to a generalized zeroth-order Tikhonov regularization^{26,41,43}. This insight provides a Bayesian rationale for the selection of residual and regularisation terms, respectively, as the negative logarithms of the likelihood and prior distributions. It also provides a rule for selecting the regularization parameter κ_j , which can be extended to anisotropic variances (see later). More generally, (11) provides a general

Bayesian regularization framework for the handling of probability distributions of any form. The Bayesian interpretation also provides access to the full Bayesian inversion apparatus, outlined in the following sections, offering many advantages over traditional regularization methods.

C. Bayesian Posterior and Model Uncertainty Quantification

It can be shown^{24,26,51–55} that the posterior (10) obtained from multivariate Gaussian likelihood and prior distributions (14)-(15) is also multivariate Gaussian:

$$p(\Xi_j | \dot{X}_j) = \mathcal{N}(\Xi_j; \hat{\Xi}_j, \hat{\Delta}_j) = \frac{\exp(-\frac{1}{2} \|\Xi_j - \hat{\Xi}_j\|_{\hat{\Delta}_j^{-1}}^2)}{\sqrt{(2\pi)^c \det(\hat{\Delta}_j)}}, \quad (17)$$

based on the c -dimensional mean vector and $c \times c$ covariance matrix, respectively:

$$\begin{aligned} \hat{\Xi}_j &= \hat{\Delta}_j (\Theta^\top V_{\epsilon_j}^{-1} \dot{X}_j + V_{\Xi_j}^{-1} \mu_j) \\ \hat{\Delta}_j &= (\Theta^\top V_{\epsilon_j}^{-1} \Theta + V_{\Xi_j}^{-1})^{-1}. \end{aligned} \quad (18)$$

This gives an analytical solution for the model coefficients $\hat{\xi}_{\ell_j} \in \hat{\Xi}_j$ in (16). Furthermore, the standard deviations $\hat{\sigma}_{\xi_{\ell_j}}$ of each coefficient $\hat{\xi}_{\ell_j}$, calculated from the square roots of diagonal terms $(\hat{\Delta}_j)_{\ell\ell}$ in the covariance matrices $\hat{\Delta}_j$, provide quantitative estimates of the error in each coefficient – thereby quantifying the model uncertainty^{29,38}.

While the matrix inversions in (18) are computationally expensive, they are quite feasible for low-dimensional problems, such as those in this study. For high-dimensional problems, the posterior mean and covariance can be computed efficiently using the optimization in (16) or (A2).

D. Bayesian Model Selection

A strong advantage of the Bayesian framework is that it enables the quantitative ranking of models. Consider two models (9) for the same data, respectively:

$$\dot{X}_j = \Theta^{(1)}(\mathbf{X})\Xi_j^{(1)} + \epsilon_j, \quad \dot{X}_j = \Theta^{(2)}(\mathbf{X})\Xi_j^{(2)} + \epsilon_j \quad (19)$$

where (1) or (2) is the model index. The models can be ranked by the ratio of their posteriors, known as the posterior odds ratio (POR)^{14,53}:

$$\text{POR}_j^{(1)/(2)} = \frac{p(\Xi_j^{(1)} | \dot{\mathbf{X}}_j)}{p(\Xi_j^{(2)} | \dot{\mathbf{X}}_j)} \quad (20)$$

If the pdfs are expressed as point values using the Bayesian MAP estimates (16), then (20) provides a useful metric for model selection (“*naive Bayes*”), with model (1) preferred for $\text{POR}_j > 1$. For Gaussian posteriors (17) within the same model class (constant c) and near-constant covariance matrices, (20) reduces to the logarithmic form:

$$\begin{aligned} \ln \text{POR}_j^{(1)/(2)} &= \ln p(\Xi_j^{(1)} | \dot{\mathbf{X}}_j) - \ln p(\Xi_j^{(2)} | \dot{\mathbf{X}}_j) \\ &\approx -\frac{1}{2} \left(\|\Xi_j - \hat{\Xi}_j^{(1)}\|_{(\hat{\Delta}_j^{(1)})^{-1}}^2 - \|\Xi_j - \hat{\Xi}_j^{(2)}\|_{(\hat{\Delta}_j^{(2)})^{-1}}^2 \right) \end{aligned} \quad (21)$$

with model (1) preferred for $\ln \text{POR}_j > 0$. For a fixed reference model, (21) can be applied in an absolute sense:

$$\ln \text{POR}_j^{(*)} \approx -\frac{1}{2} \|\Xi_j - \hat{\Xi}_j^{(*)}\|_{(\hat{\Delta}_j^{(*)})^{-1}}^2 \quad (22)$$

The maximization of (22) therefore provides a quantitative rule for model selection, equivalent for the assumptions made here to minimization of the posterior Gaussian norm.

E. Bayesian Evidence

A further advantage of the Bayesian apparatus is that the evidence $p(\dot{\mathbf{X}}_j)$ in Bayes’ rule (10) – sometimes termed the prior predictive distribution or marginal distribution – provides a measure of the goodness of fit of the model to the data^{15,52}. For the analysis here, since the likelihood, prior and posterior are multivariate Gaussian, the evidence is also multivariate Gaussian^{52,54,55}:

$$p(\dot{\mathbf{X}}_j) = \mathcal{N}(\dot{\mathbf{X}}_j; \hat{\mathbf{X}}_j, \hat{\Omega}_j) = \frac{\exp(-\frac{1}{2} \|\dot{\mathbf{X}}_j - \hat{\mathbf{X}}_j\|_{\hat{\Omega}_j^{-1}}^2)}{\sqrt{(2\pi)^m \det(\hat{\Omega}_j)}}, \quad (23)$$

with the m -dimensional mean vector and $m \times m$ covariance matrix for each dimension:

$$\begin{aligned} \hat{\mathbf{X}}_j &= \Theta \boldsymbol{\mu}_j = \mathbf{0} \\ \hat{\Omega}_j &= \Theta \mathbf{V}_{\Xi_j} \Theta^\top + \mathbf{V}_{\epsilon_j} \end{aligned} \quad (24)$$

Thus for the Gaussian assumptions made in this study, the evidence can be calculated analytically. However, this requires the inversion of potentially large $m \times m$ covariance matrices $\hat{\Omega}_j$, which introduce computational difficulties. For this reason, Bayesian practitioners usually use exploratory numerical methods such as Markov chain Monte Carlo (MCMC)^{15,42,51,52} or nested sampling⁵⁶ to explore the shape of the posterior and compute the evidence.

F. Extended Bayesian Regularization with Nuisance Parameters

The Bayesian regularization method in §II B assumes multivariate Gaussian distributions for the error (12)-(14) and prior (15), with specified covariance matrices \mathbf{V}_{ϵ_j} and \mathbf{V}_{Ξ_j} , respectively. In most situations these matrices are *a priori* not known. Their estimation as nuisance parameters can in fact be incorporated into the Bayesian framework. Consider the joint posterior pdf $p(\Xi_j, \mathbf{V}_{\epsilon_j}, \mathbf{V}_{\Xi_j} | \dot{\mathbf{X}}_j)$ of the model and unknown matrices, subject to the data. Applying Bayes' rule:

$$p(\Xi_j, \mathbf{V}_{\epsilon_j}, \mathbf{V}_{\Xi_j} | \dot{\mathbf{X}}_j) = \frac{p(\dot{\mathbf{X}}_j | \Xi_j, \mathbf{V}_{\epsilon_j}, \mathbf{V}_{\Xi_j}) p(\Xi_j, \mathbf{V}_{\epsilon_j}, \mathbf{V}_{\Xi_j})}{p(\dot{\mathbf{X}}_j)} \quad (25)$$

By separation of the prior $p(\Xi_j, \mathbf{V}_{\epsilon_j}, \mathbf{V}_{\Xi_j}) = p(\Xi_j | \mathbf{V}_{\epsilon_j}, \mathbf{V}_{\Xi_j}) p(\mathbf{V}_{\epsilon_j}) p(\mathbf{V}_{\Xi_j})$ for independent covariance matrices, and using the simplifications $p(\Xi_j | \mathbf{V}_{\epsilon_j}, \mathbf{V}_{\Xi_j}) = p(\Xi_j | \mathbf{V}_{\Xi_j})$ (independence of the model from the noise) and $p(\dot{\mathbf{X}}_j | \Xi_j, \mathbf{V}_{\epsilon_j}, \mathbf{V}_{\Xi_j}) = p(\dot{\mathbf{X}}_j | \Xi_j, \mathbf{V}_{\epsilon_j})$ (independence of the data from the prior), (25) simplifies to:

$$p(\Xi_j, \mathbf{V}_{\epsilon_j}, \mathbf{V}_{\Xi_j} | \dot{\mathbf{X}}_j) = \frac{p(\dot{\mathbf{X}}_j | \Xi_j, \mathbf{V}_{\epsilon_j}) p(\Xi_j | \mathbf{V}_{\Xi_j}) p(\mathbf{V}_{\epsilon_j}) p(\mathbf{V}_{\Xi_j})}{p(\dot{\mathbf{X}}_j)} \quad (26)$$

To simplify (26), we again choose Gaussian likelihood and prior distributions (14)-(15), based on anisotropic diagonal error and model covariance matrices:

$$\begin{aligned} \mathbf{V}_{\epsilon_j} &= \text{diag}[\mathbf{v}_{\epsilon_j}] \quad \text{with} \quad \mathbf{v}_{\epsilon_j} = [v_{\epsilon_{1j}}, \dots, v_{\epsilon_{ij}}, \dots, v_{\epsilon_{mj}}]^\top \\ \mathbf{V}_{\Xi_j} &= \text{diag}[\mathbf{v}_{\Xi_j}] \quad \text{with} \quad \mathbf{v}_{\Xi_j} = [v_{\Xi_{1j}}, \dots, v_{\Xi_{\ell j}}, \dots, v_{\Xi_{cj}}]^\top \end{aligned} \quad (27)$$

where diag maps a vector to the diagonal of a matrix. The conjugate priors for the covariance matrices $p(\mathbf{V}_{\epsilon_j})$ and $p(\mathbf{V}_{\Xi_j})$ are assumed separable, given by the product of individual Inverse

Gamma (IG) distributions:

$$\begin{aligned}
 p(\mathbf{V}_{\epsilon_j}) &= p(\mathbf{v}_{\epsilon_j}) = \prod_{i=1}^m p(v_{\epsilon_{ij}}) = \prod_{i=1}^m \text{IG}(v_{\epsilon_{ij}}; \alpha_{\epsilon_{ij}}, \beta_{\epsilon_{ij}}) \\
 p(\mathbf{V}_{\Xi_j}) &= p(\mathbf{v}_{\Xi_j}) = \prod_{\ell=1}^c p(v_{\Xi_{\ell j}}) = \prod_{\ell=1}^c \text{IG}(v_{\Xi_{\ell j}}; \alpha_{\Xi_{\ell j}}, \beta_{\Xi_{\ell j}})
 \end{aligned} \tag{28}$$

in which $\{\alpha_\iota, \beta_\iota\}$ for $\iota \in \{\epsilon_{ij}, \Xi_{\ell j}\}$ are the shape and scale hyperparameters, respectively. The IG distribution can be derived as the marginal posterior distribution for an unknown variance of a Gaussian distribution with an uninformative prior^{57,58}, and is commonly used for variance estimation in Bayesian inference. It can be interpreted as a two-parameter positive generalization of the Student's t -distribution with a small positive peak and heavy tail, with the mean and variance²³:

$$\mathbf{E}_\iota = \mathbb{E}[v_\iota] = \frac{\beta_\iota}{\alpha_\iota - 1}, \quad \text{for } \alpha_\iota > 1 \tag{29}$$

$$\mathbf{V}_\iota = \text{Var}[v_\iota] = \frac{\beta_\iota^2}{(\alpha_\iota - 1)^2(\alpha_\iota - 2)} \quad \text{for } \alpha_\iota > 2. \tag{30}$$

The IG hyperparameters $\{\alpha_\iota, \beta_\iota\}$ or alternatively $\{\mathbf{E}_\iota, \mathbf{V}_\iota\}$ can be chosen based on prior belief or experience, or computed iteratively until a convergence criterion is achieved.

To compute the joint posterior (26) with the conjugate priors (28), two algorithms are commonly used²³:

- The *joint maximum a posteriori* (JMAP) method, defined by the logarithmic optimization²³:

$$(\hat{\Xi}_j^{\text{JMAP}}, \hat{\mathbf{V}}_{\epsilon_j}^{\text{JMAP}}, \hat{\mathbf{V}}_{\Xi_j}^{\text{JMAP}}) \tag{31}$$

$$= \arg \max_{\Xi_j, \mathbf{V}_{\epsilon_j}, \mathbf{V}_{\Xi_j}} [\ln p(\Xi_j, \mathbf{V}_{\epsilon_j}, \mathbf{V}_{\Xi_j} | \dot{\mathbf{X}}_j)] \tag{32}$$

This can be implemented iteratively using the analytical solution (18), for which the pseudocode of an algorithm has been reported²³.

- The *variational Bayes approximation* (VBA) method, which approximates the posterior by the separable distribution $q(\Xi_j, \mathbf{V}_{\epsilon_j}, \mathbf{V}_{\Xi_j}) = q_1(\Xi_j)q_2(\mathbf{V}_{\epsilon_j})q_3(\mathbf{V}_{\Xi_j})$ using the Gaussian prior (15) for q_1 and IG conjugate priors (28) for q_2 and q_3 . These can be computed iteratively by minimizing the Kullback-Leibler divergence between $p(\Xi_j, \mathbf{V}_{\epsilon_j}, \mathbf{V}_{\Xi_j} | \dot{\mathbf{X}}_j)$ and q , for which the pseudocode of an algorithm has been reported²³.

G. Other Model Selection Metrics

Many other metrics have also been proposed for model selection by traditional or Bayesian methods. These include the Akaike information criterion (AIC) and Bayes information criterion (BIC), respectively⁵⁹:

$$\begin{aligned} \text{AIC}_j &= -2 \ln p(\dot{\mathbf{X}}_j | \hat{\boldsymbol{\Xi}}_j) + 2c \\ \text{BIC}_j &= -2 \ln p(\dot{\mathbf{X}}_j | \hat{\boldsymbol{\Xi}}_j) + c \ln m \end{aligned} \quad (33)$$

where $\ln p(\dot{\mathbf{X}}_j | \hat{\boldsymbol{\Xi}}_j)$ is the maximized log-likelihood based on the estimated coefficients $\hat{\boldsymbol{\Xi}}_j$. For finite sample sizes, AIC_j requires a correction given by⁴:

$$\text{AIC}_j^c = \text{AIC}_j + \frac{2(c+1)(c+2)}{m-c-2} \quad (34)$$

Some authors^{4,59} have approximated 2-norm forms of the AIC and BIC based on $\ln p(\dot{\mathbf{X}}_j | \hat{\boldsymbol{\Xi}}_j) \approx -\frac{m}{2} \ln(\|\dot{\mathbf{X}}_j - \boldsymbol{\Theta}(\mathbf{X})\boldsymbol{\Xi}_j\|_2^2/m)$. An alternative metric is the ‘‘error bar’’, defined as the sum of squared coefficients of variation of the posterior^{28,31}:

$$\text{EB}_j = \sum_{\substack{\ell=1 \\ \hat{\xi}_{\ell j} \neq 0}}^c \frac{(\hat{\Delta}_j)_{\ell\ell}}{\hat{\xi}_{\ell j}^2} \quad (35)$$

It is claimed³¹ that this should be minimized to choose models with lower variance.

III. APPLICATIONS TO DYNAMICAL SYSTEMS

A. Dynamical Systems and Methodology

To compare the traditional and Bayesian methods for dynamical system identification, three dynamical systems were analyzed by the SINDy, JMAP and VBA algorithms:

- (a) The Lorenz system, a simplified two-dimensional atmospheric convection system given by^{60,61}:

$$\dot{\mathbf{x}} = [\sigma(y - x), x(\rho - z) - y, xy - \beta z]^\top \quad (36)$$

The parameter values $[\sigma, \rho, \beta] = [10, \frac{8}{3}, 28]$ give chaotic behavior.

- (b) The Vance system, a one-predator two-prey ecological system given by^{62,63}:

$$\dot{\mathbf{x}} = (\mathbf{r} - \boldsymbol{\alpha}\mathbf{x}) \odot \mathbf{x} \quad (37)$$

where \odot is the element-wise (Hadamard) vector product. The parameter values $\mathbf{r} = \begin{bmatrix} 1 \\ 1 \\ -1 \end{bmatrix}$ and $\boldsymbol{\alpha} = \frac{1}{1000} \begin{bmatrix} 1 & 1 & 10 \\ 1.5 & -0.5 & 0 \end{bmatrix}$ give chaotic behavior.

(c) The Shil'nikov system, a cubic modification of the Lorenz system given by^{61,64}:

$$\dot{\mathbf{x}} = [y, x(1 - z) - Bx^3 - \lambda y, -\alpha(z - x^2)]^\top \quad (38)$$

The parameter values $[\alpha, \lambda, B] = \left[\frac{4\sqrt{30}}{135}, \frac{11\sqrt{30}}{90}, \frac{2}{13} \right]$ give chaotic behavior.

Phase plots of these systems with added noise (see below) are shown in Figures 1(a)-(c). The analyses were primarily conducted in MATLAB 2021b on a MacBook Pro with 2.3 GHz Intel Core i9, with numerical integration by the ode45 function. For each system, the data \mathbf{X} were calculated and then augmented by additive random noise, drawn from a standard normal distribution multiplied by a scaling parameter ε . The noise-moderated derivative data $\dot{\mathbf{X}}$ were then recalculated from the noisy data by a dynamical system call. For the regularization process, an alphabet was selected to construct $\Theta(\mathbf{X})$, with the possibility of linear, polynomial (up to third order) and other functions. The main code computes the dynamical system, and then calls the SINDy algorithm^{1,4} and modified forms of the JMAP and VBA algorithms²³, each using an inner iteration at selected value(s) of λ or $\{\alpha_\iota, \beta_\iota\}$ for $\iota \in \{\epsilon_{ij}, \Xi_{\ell j}\}$ – for the Bayesian algorithms using a convergence criterion for $\ln \det \hat{\Delta}_j^{-1}$ – and an outer iteration to explore changes in one or more of these (hyper)parameters. In this study, the prior (15) hyperparameters $\{\alpha_{\Xi_{\ell j}}, \beta_{\Xi_{\ell j}}\}$ were fixed to give a broad Gaussian distribution – expressing a consistent degree of belief in the expected model coefficients – while the outer iterations were conducted over the likelihood (14) hyperparameters $\{\alpha_{\epsilon_{ij}}, \beta_{\epsilon_{ij}}\}$ as expressed by the IG mean $\mathbf{E}_{\epsilon_{ij}}$ (30), to discover the error in the data. This iteration sequence is shown in Figure 1(d), proceeding right to left. The code also makes subroutine or function calls to a number of utility files^{1,4,23,32} for the purpose of analyzing, plotting and exporting the data.

For the Bayesian algorithms, the code calculates the mean and covariance estimators for the posterior (18) and evidence (24), and the Gaussian norms within the likelihood (14), prior (15), posterior (17) and evidence (23). Attempts were made to calculate the full Gaussian distributions for the posterior (17) and evidence (23), using the logdet function⁶⁵ for the denominator determinant terms, but these were affected by numerical underflow in many instances. Some numerical difficulties were also encountered in the evidence Gaussian norms.

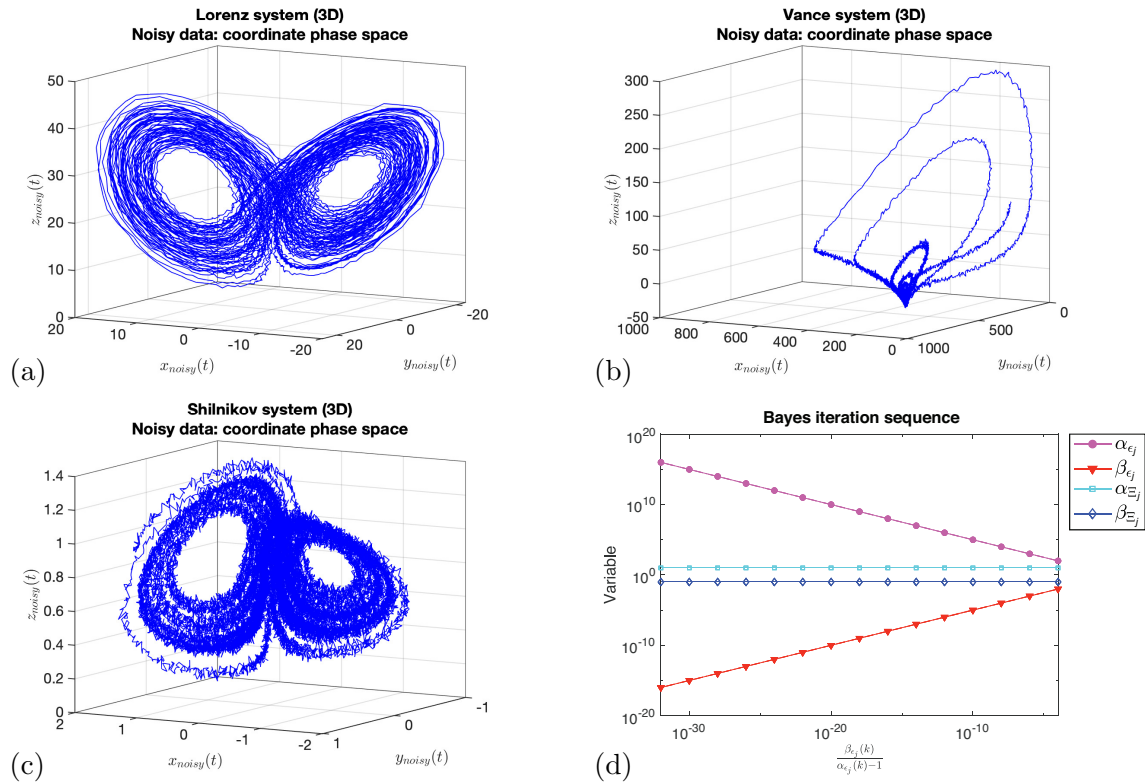


FIG. 1. Phase plots of noisy data for dynamical systems in this study: (a) Lorenz system with $\varepsilon = 0.2$; (b) Vance system with $\varepsilon = 2.0$; (c) Shil'nikov system with $\varepsilon = 0.02$; and (d) outer iteration sequence used for the JMAP and VBA algorithms (from right to left).

The code also computes the metrics defined in (33)-(35) and their 2-norm approximations³².

B. Results

The analyses are illustrated in Figures 2-6, with more complete sets of graphs in the Supplementary Information. A number of graphs are presented for each system, as follows:

- For all algorithms, plots are provided of 2-norms including the residual terms $\|\dot{\mathbf{X}}_j - \Theta \Xi_j\|_2^2$ (dark blue), regularization terms $\|\Xi_j\|_2^2$ (red) and objective functions $J_j = \|\dot{\mathbf{X}}_j - \Theta \Xi_j\|_2^2 + \psi \|\Xi_j\|_2^2$ (7) (black), using $\psi = \lambda$ for SINDy and $\psi = \kappa_j = \min(\bar{\mathbf{v}}_{\epsilon_j} \mathbf{1} \odot \mathbf{v}_{\Xi_j})$ for JMAP and VBA, where $\bar{\mathbf{v}}_{\epsilon_j}$ is the mean \mathbf{v}_{ϵ_j} , $\mathbf{1}$ is the 1 vector and \odot is the element-wise division operator. These are plotted to show the outer iteration sequence, for SINDy against the regularization parameter λ , and for JMAP and VBA against $\mathbf{E}_{\epsilon_{ij}} = \beta_{\epsilon_{ij}} / (\alpha_{\epsilon_{ij}} - 1)$ (30).

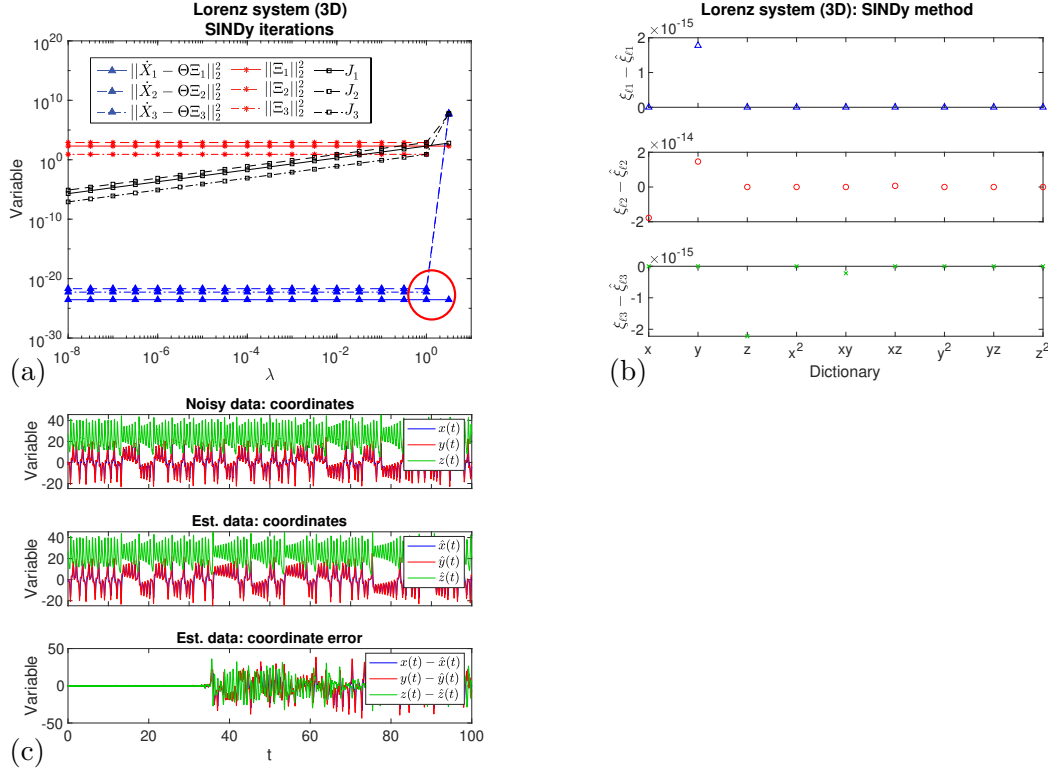


FIG. 2. Lorenz system, SINDy regularization with $t = 100$, $t_{step} = 0.01$, $\varepsilon = 0.2$: (a) plots of 2-norm residual, regularization and objective functions (7) with decreasing λ , showing the optimal iteration; (b) optimal error in predicted coefficients $\xi_{\ell_j} - \hat{\xi}_{\ell_j}$; and (c) original and optimal predicted data and their differences.

- For JMAP and VBA, plots are provided of Gaussian norms for the likelihood $\|\dot{\mathbf{X}}_j - \Theta \Xi_j\|_{\mathbf{V}_{\epsilon_j}^{-1}}^2$ (medium blue), prior $\|\Xi_j\|_{\mathbf{V}_{\epsilon_j}^{-1}}^2$ (pink), posterior $\|\Xi_j - \hat{\Xi}_j\|_{\hat{\Delta}_j^{-1}}^2$ (green) and evidence $\|\dot{\mathbf{X}}_j - \hat{\mathbf{X}}_j\|_{\hat{\Omega}_j^{-1}}^2 = \|\dot{\mathbf{X}}_j\|_{\hat{\Omega}_j^{-1}}^2$ by direct calculation (orange) or from Bayes' rule (slate blue). These are plotted against $\mathbf{E}_{\epsilon_{ij}}$.
- For all algorithms, plots are provided of the differences between the true and optimal predicted model coefficients $\xi_{\ell_j} - \hat{\xi}_{\ell_j}$, over the alphabet of functions used. These show the precision of the predicted coefficients. For the Bayesian algorithms, they allow the error bars on each coefficient to be illustrated clearly.
- For all algorithms, a triple plot is provided of the noisy time-series data, the predicted data (using the optimal coefficients) and their differences. These illustrate the degree of success of the inference method used.

The Lorenz system with added noise is illustrated in Figure 1(a). The SINDy, JMAP and VBA analyses are shown respectively in Figures 2-4 and S1-S4, and the metrics in Figures S3-S5. As shown:

- The SINDy algorithm rapidly finds an optimal solution with decreasing λ ; this is somewhat ambiguous but can be assigned to the turning point in the 2-norm residual (Figure 2(a)). The calculated coefficients have a precision of $\sim 10^{-14}$ to 10^{-15} (Figure 2(b)), with excellent recovery of the time series to $t \approx 35$ (Figure 2(c)).
- In contrast, the JMAP and VBA algorithms converge more slowly with decreasing $E_{\epsilon_{ij}}$, but both find optimal solutions, identified by the minimum posterior Gaussian norm in (17) (Figures 3 and 4, (b) and (f))). This is equivalent to the maximum absolute log POR (22), and clearly illustrates the operation of the Bayesian MAP method. For the constant conjugate priors used in this study, each optimum also corresponds to the minimum in the likelihood Gaussian norm. They also correspond to (or are close to) the turning points in the 2-norm residuals (Figures 3 and 4(a) and (e)).
- For the JMAP and VBA algorithms, the evidence norms were approximately constant, with some numerical dispersion evident at low values of $E_{\epsilon_{ij}}$. This supports the assumption made in the derivation of the MAP estimator in (11).
- The JMAP and VBA algorithms also provide error bars on the predicted coefficients (Figures 3 and 4(c) and (g)), extracted from the posterior covariance matrix (Section II C). The calculated errors are $\sim 10^{-7}$, much larger than the SINDy precision. The time windows for recovery of the time series are similar to the SINDy method. Together, these suggest overfitting of the data by the SINDy algorithm, to an unjustifiably high precision.
- The model selection metrics AIC and BIC (33) do not provide any discernible optima for either JMAP or VBA (Figures S3(a) and S5(a)). The EB (35) does exhibit an optimum solution, but contrary to previous arguments³¹, this corresponds to the point of maximum rather than minimum variance. The 2-norm variants AIC_2 , AIC_2^c and BIC_2 (Figures S3(b) and S5(b)) reveal an optimum, but this corresponds to the turning point of the 2-norm residual, obviating any need for these metrics.

Examining the effect of different parameter choices on the JMAP and VBA analyses of

Dynamical System Identification by Bayesian Inference

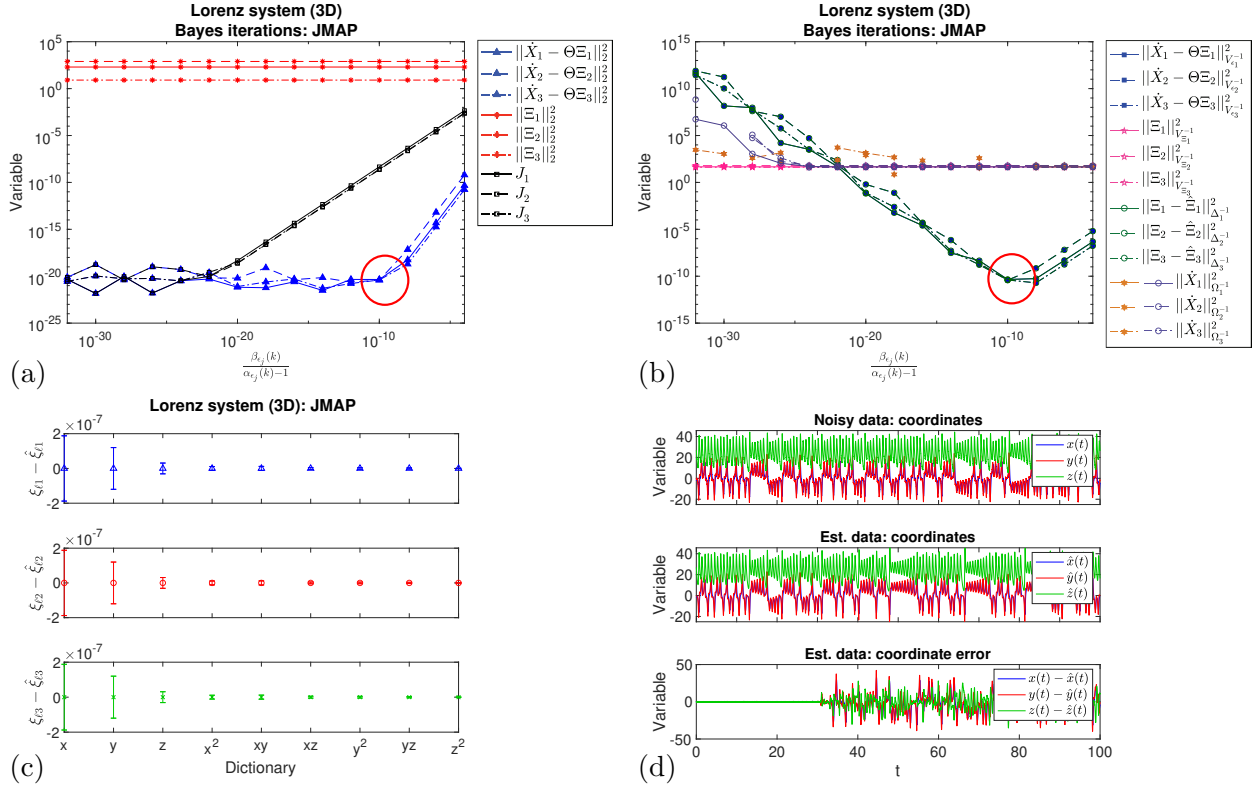


FIG. 3. Lorenz system, JMAP regularization with $t = 100$, $t_{step} = 0.01$, $\varepsilon = 0.2$: (a) iteration sequence with decreasing $E_{e_{ij}}$, showing the 2-norm residual, regularization and objective functions (7) and the optimal iteration; (b) Gaussian norms for the prior, likelihood, posterior and evidence, showing the optimal iteration; (c) optimal error in predicted coefficients $\xi_{\ell_j} - \hat{\xi}_{\ell_j}$, with error bars calculated from the posterior covariance (18); and (d) original and optimal predicted data and their differences.

the Lorenz system:

- The effect of length of the time-series training data – expressed by the number of data points m – on the absolute coefficient errors $|\xi_{\ell_j} - \hat{\xi}_{\ell_j}|$ is shown in Figure 5(a), with supporting data for JMAP shown in Figure S6. As shown, the errors increase with fewer data points, but remain quite acceptable for time series from 10000 points down to 10 points, sharply rising only for time series with less than 10 points. The JMAP algorithm was found to be more robust to smaller data sets. If applicable generally, the results support the viability of real-time applications of Bayesian inference to incoming dynamical system data.
- For the above examples at low m , breakdown of the JMAP and VBA algorithms is

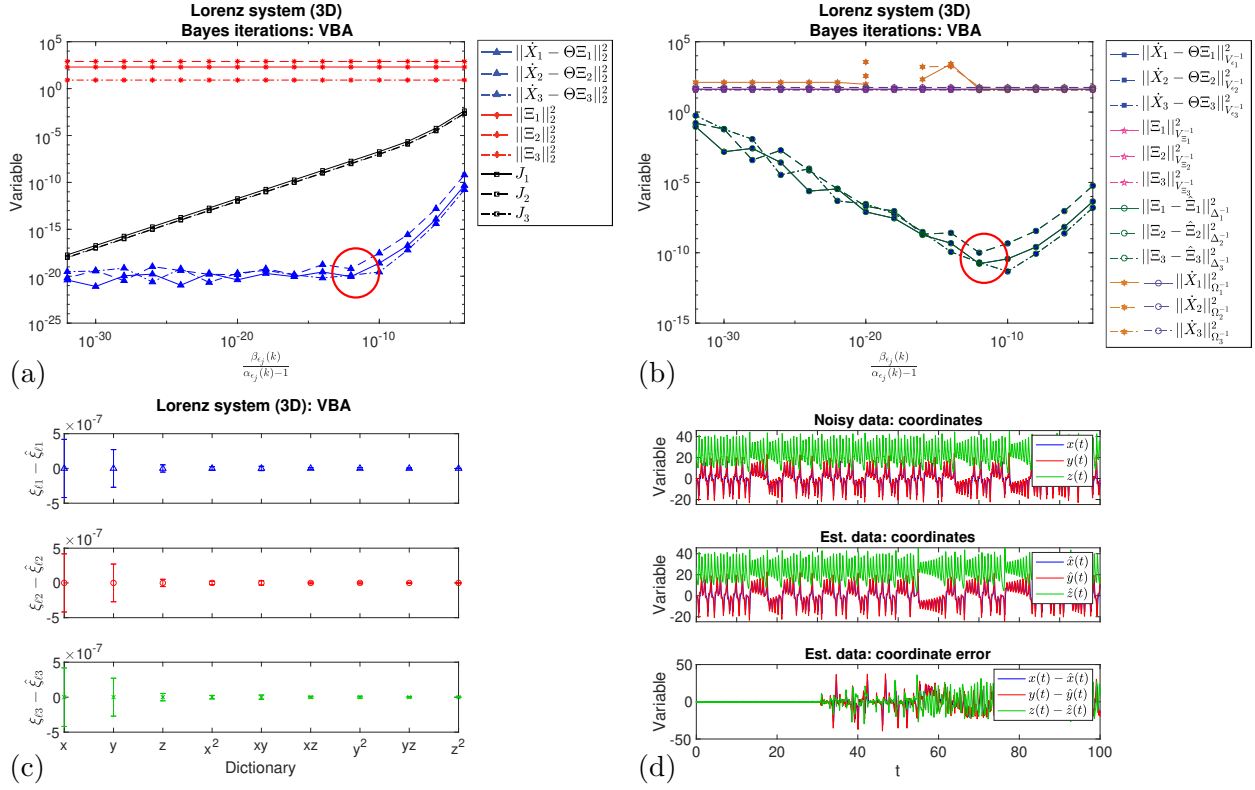


FIG. 4. Lorenz system, VBA regularization with $t = 100$, $t_{step} = 0.01$, $\varepsilon = 0.2$: (a) iteration sequence with decreasing $E_{e_{ij}}$, showing the 2-norm residual, regularization and objective functions (7) and the optimal iteration; (b) Gaussian norms for the prior, likelihood, posterior and evidence, showing the optimal iteration; (c) optimal error in predicted coefficients $\xi_{lj} - \hat{\xi}_{lj}$, with error bars calculated from the posterior covariance (18); and (d) original and optimal predicted data and their differences.

revealed by (i) very large error bars on some predicted coefficients (e.g., Figure S6(e)); (ii) separation of the likelihood and posterior Gaussian norms (e.g., Figure S6(f)), which should follow similar trends for a constant prior; (iii) unexpected changes in the evidence Gaussian norm; and/or (iv) negative diagonal terms in the posterior covariance matrix $\hat{\Delta}_j$, giving complex standard deviations $\hat{\sigma}_{\xi_{lj}}$. In contrast, the SINDy method exhibits a turning point in its 2-norm residual, implying the existence of a solution, without giving any indication that something is amiss.

- The effect of added Gaussian noise – expressed by the parameter ε – is shown in Figure 5(b). Unexpectedly, the error decreases with larger added noise. Some differences were evident between the JMAP and VBA algorithms.

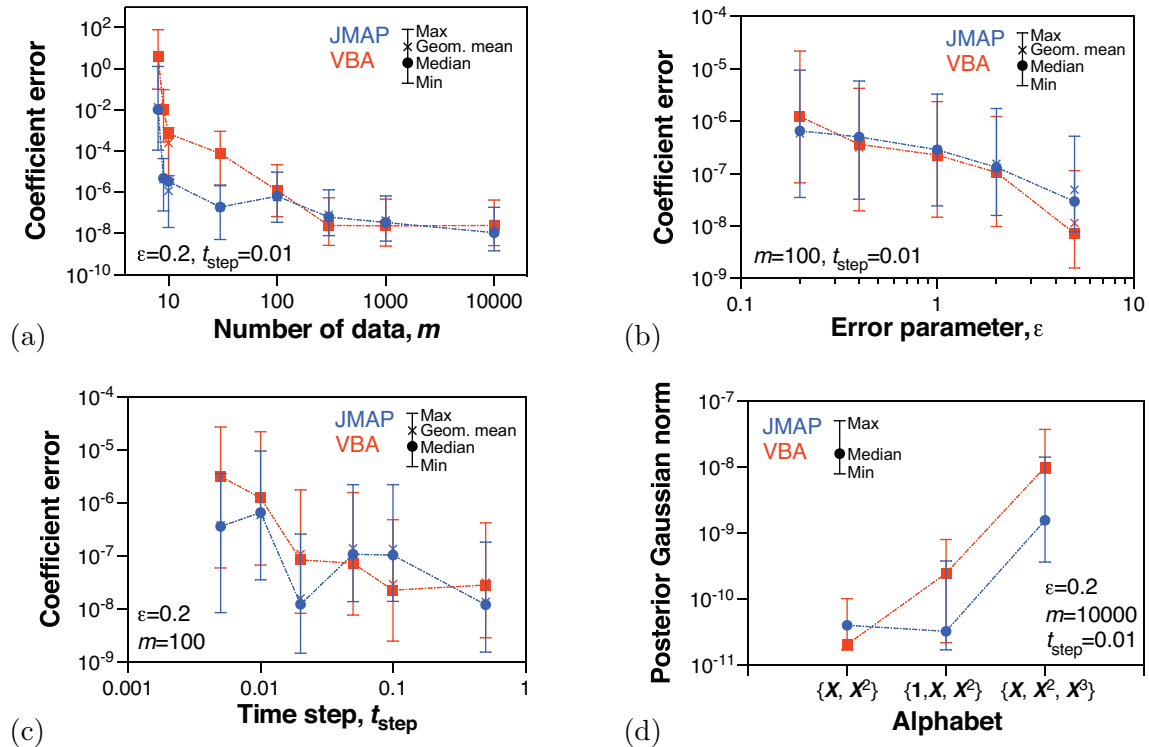


FIG. 5. Lorenz system, effect of parameters on JMAP and VBA algorithms: (a) training data length; (b) added noise; (c) time step interval; and (d) choice of alphabet.

- The effect of the time step interval, for data series of the same length m , is shown in Figure 5(c). These data broadly indicate that the coefficient errors decrease with larger time steps, but with some fluctuations, presumably due to interactions between the step interval and intrinsic timescales of the Lorenz system.
- The effect of different choices of alphabet, including second-order polynomials with a column of 1s, or third-order polynomials, is shown in Figure 5(d), with supporting data for JMAP shown in Figure S7. As shown, the inclusion of unnecessary functions in the alphabet produces larger error bars on the predicted coefficients. It is also revealed by higher posterior Gaussian norms.
- Different processors (Mac Intel 8-core or 4-core) were found to give small differences in the 2-norm residuals and posterior Gaussian norms, especially for large data sets or at low values of $E_{\epsilon_{ij}}$, but these did not affect the choice of optimal iterations, the predicted coefficients or the main conclusions.

The Vance system with added noise is illustrated in Figure 1(b), and the analyses in

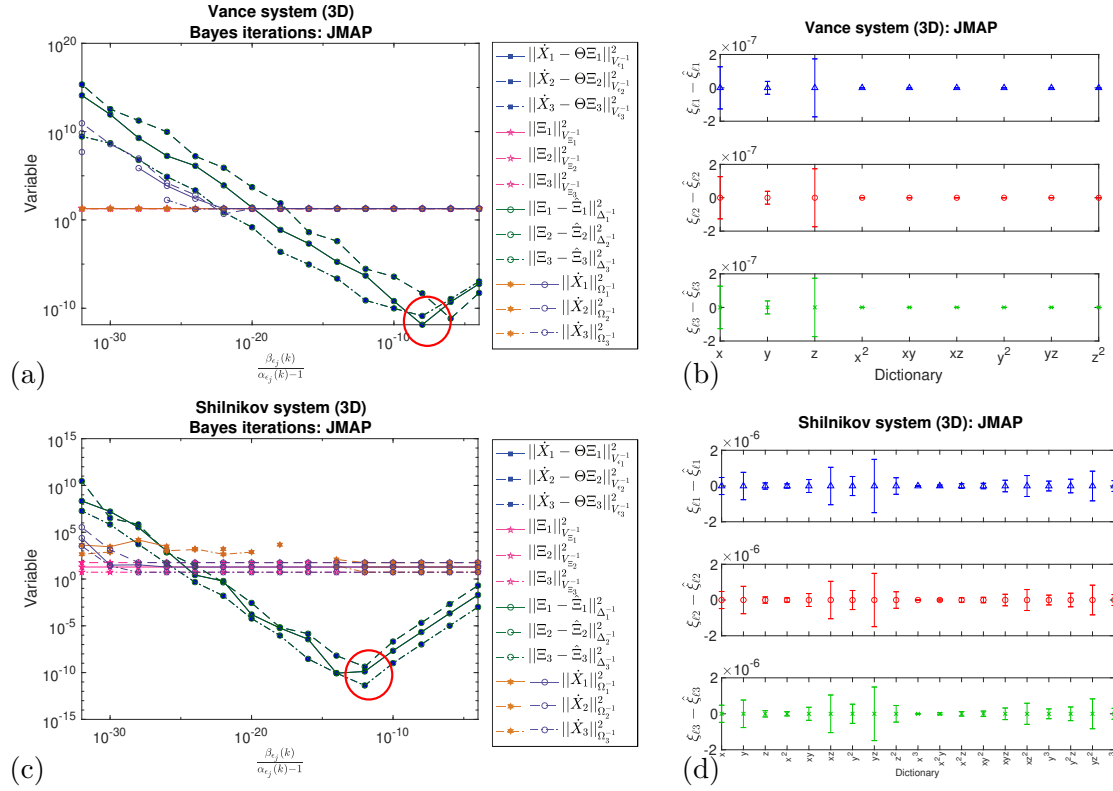


FIG. 6. Vance (a)-(b) and Shil'nikov (c)-(d) systems with $t = 500$, $t_{step} = 0.02$, showing JMAP regularization: (a),(c) Gaussian norms for the prior, likelihood, posterior and evidence, with the optimal iteration; (b),(d) optimal error in predicted coefficients $\xi_{\ell_j} - \hat{\xi}_{\ell_j}$, with error bars calculated from the posterior covariance (18).

Figures 6(a)-(b) and S8-S12. Here the SINDy algorithm requires more iterations to find the optimum, due to the presence of small coefficients. Otherwise, the three algorithms are broadly similar to the Lorenz system. The JMAP and VBA optima are again identified by the minimum posterior norms, corresponding to a turning points in the 2-norm residuals. The Bayesian methods give coefficient errors of $\sim 10^{-6}$ to 10^{-7} , much higher than the SINDy precision ($\sim 10^{-15}$ to 10^{-16}).

The Shil'nikov system with added noise is illustrated in Figure 1(c), and the analyses in Figures 6(c)-(d) and S13-S17. Despite requiring a third-order polynomial alphabet, the three algorithms behave similarly to the Lorenz system, with optimal coefficient errors of $\sim 10^{-6}$. For this system, the Bayesian algorithms infer significant error bars for many coefficients.

IV. CONCLUSIONS

This study presents a maximum *a posteriori* (MAP) Bayesian framework for the identification of a dynamical system (1) from its discrete time series data. For Gaussian multivariate prior and likelihood distributions, the MAP estimate of the posterior distribution is shown to be equivalent to a generalized zeroth-order Tikhonov regularization (§II B), providing a rational justification for the choice of the residual and regularization terms, respectively, from the negative logarithms of the likelihood and prior distributions. The Bayesian regularization can be used to infer a matrix of model coefficients associated with an alphabet of functions of the data, to reproduce the dynamical system very precisely. The Bayesian interpretation also gives access to the full apparatus for Bayesian inference, including the Bayesian posterior and model uncertainty quantification (§II C), the posterior Bayes factor and Bayesian model selection (§II D), the Bayesian evidence (§II E), and the JMAP and VBA algorithms for the estimation of unknown hyperparameters (§II F). In §III, the JMAP and VBA algorithms are applied to the analysis of three dynamical systems with added noise, in comparison to the well-known SINDy algorithm for thresholded least-squares regression¹.

From the theoretical analyses and the three case studies, the following conclusions can be drawn:

- The assumption of multivariate Gaussian likelihood (14) and prior (15) distributions – while not required for Bayesian inference – enables a dramatic simplification of Bayes’ rule (10), to give multivariate Gaussian posterior (17) and evidence (23) distributions. This gives the closed-form analytical solutions (18) and (24), simplifying the construction of MAP algorithms and computations for low-dimensional data.
- The Mahalanobis distance $\|\Xi_j - \hat{\Xi}_j\|_{\hat{\Delta}_j}^2$, extracted from (17) and referred to as the “posterior Gaussian norm”, provides a point estimate of the posterior distribution (17). Its minimization corresponds to maximization of the absolute log posterior odds ratio (22) based on the MAP estimate, for systems with a fixed alphabet, fixed data length and near-constant prior and likelihood covariances. As demonstrated by the three case studies, the posterior Gaussian norm provides a robust metric for Bayesian model selection, giving a clearly defined minimum for iterations over the error hyperparameters.
- For JMAP and VBA iterations using constant prior hyperparameters, the minimum pos-

terior Gaussian norm corresponds to the minimum likelihood Gaussian norm $\|\dot{\mathbf{X}}_j - \Theta \Xi_j\|_{\mathbf{V}_{\epsilon_j}^{-1}}^2$. It also corresponds to (or is close to) a turning point in the 2-norm residual $\|\dot{\mathbf{X}}_j - \Theta \Xi_j\|_2^2$. For SINDy iterations, the optimal value of the threshold λ can also be assigned to this turning point, no other metric being available.

- Contrary to the suggestions of many Bayesian practitioners^{15,54,55}, the evidence distribution (23) – represented by the evidence Gaussian norm $\|\dot{\mathbf{X}}_j - \hat{\mathbf{X}}_j\|_{\hat{\Omega}_j^{-1}}^2$ point estimate – was relatively constant (or was subject to numerical problems) over the hyperparameter choices examined. It was therefore not relevant for Bayesian model selection.
- The model selection metrics AIC and BIC (33) and their 2-norm counterparts do not incorporate the Bayesian prior, and so must be interpreted as maximum likelihood rather than Bayesian metrics. For the case studies examined, no benefit was gained by their calculation. In contrast, the MAP solution corresponds to a maximum in the error bar metric (35), at the position of maximum variance.
- The Bayesian framework also enables uncertainty quantification in the predicted model coefficients, expressed as standard deviations extracted from the posterior covariance matrix (18). This is an important advantage of the Bayesian framework over traditional regularization methods^{29,38}. Analyses of the three dynamical systems indicates coefficient errors of $\sim 10^{-6}$ to 10^{-7} for time-series of length $m = 10000$, much larger than the precision ($\sim 10^{-15}$) reported by SINDy, for comparable time windows of predictability. This suggests overfitting of the data by the SINDy algorithm.
- Sensitivity analysis of the Bayesian computations indicate that the coefficient errors decrease with increasing training data length m , added Gaussian noise scale ϵ and time step interval t_{step} , and increase with unnecessarily longer alphabets (Figure 5). These trends can be used to optimize these parameters to reduce the computational cost, yet achieve a specified uncertainty. Furthermore, the coefficient errors remain acceptable ($\sim 10^{-5}$) using JMAP for Lorenz time-series down to only 10 points, suggesting the possibility of real-time applications of Bayesian inference to incoming streams of dynamical system data.
- For the analyses of the Lorenz system, the JMAP and VBA algorithms exhibit visible signs of breakdown for short time series, including (i) large coefficient errors; (ii) separation of the likelihood and posterior Gaussian norms; (iii) inconsistencies in the ev-

idence Gaussian norm; and/or (iv) complex standard deviations. In contrast, the SINDy algorithm gives solutions for the model coefficients for short time series, without any indication of computational problems.

Further research is required on the Bayesian regularization framework developed herein, as part of a broader program for the implementation of Bayesian inference for all data analysis problems throughout science and engineering. This includes deeper theoretical insights into the MAP solution and the Bayesian posterior and evidence norms, and the possibility of non-Gaussian prior or likelihood distributions and alternative conjugate priors for different dynamical systems³³. The role of the evidence norm in Bayesian model selection under the MAP framework requires further investigation. The outer iterative scheme given here can also be extended into a more elaborate optimisation method, to allow for more complicated hyperparametric representations or posterior distributions with complicated landscapes. The connections between the present MAP framework and related Bayesian methods should be examined in more detail, including functional fitting using Gaussian processes^{34–37}, latent variable or structure discovery^{66,67}, and exploratory analyses of the posterior and evidence distributions^{15,38,39,56}.

ACKNOWLEDGMENTS

The first author benefited from funding and travel support from UNSW, Canberra, Australia; Institute Pprime / CNRS / Université de Poitiers, Chasseneuil-du-Poitou, France; CentraleSupélec, Gif-sur-Yvette, France and Ambrosys GmbH, Potsdam, Germany.

Appendix A: Equivalence of Bayesian MAP Estimation and Traditional Regularization

The negative logarithm of Bayes’ rule (10) provides the general objective function for minimization in Bayesian inference:

$$\begin{aligned}
 J^B(\Xi_j) &= -\ln p(\Xi_j | \dot{\mathbf{X}}_j) \\
 &= -\ln p(\dot{\mathbf{X}}_j | \Xi_j) - \ln p(\Xi_j) + \ln p(\dot{\mathbf{X}}_j)
 \end{aligned}
 \tag{A1}$$

For the assumptions of multivariate Gaussian noise (12)-(14), prior (15) and evidence (23) made herein, with the analytical solution for the evidence (24), this reduces to:

$$\begin{aligned}
 J^B(\Xi_j) &= -\ln \frac{\exp\left(-\frac{1}{2}\|\epsilon_j\|_{\mathbf{V}_{\epsilon_j}^{-1}}^2\right)}{\sqrt{(2\pi)^m \det(\mathbf{V}_{\epsilon_j})}} - \ln \frac{\exp\left(-\frac{1}{2}\|\Xi_j\|_{\mathbf{V}_{\Xi_j}^{-1}}^2\right)}{\sqrt{(2\pi)^c \det(\mathbf{V}_{\Xi_j})}} \\
 &\quad + \ln \frac{\exp\left(-\frac{1}{2}\|\dot{\mathbf{X}}_j - \hat{\mathbf{X}}_j\|_{\hat{\Omega}_j^{-1}}^2\right)}{\sqrt{(2\pi)^m \det(\hat{\Omega}_j)}}, \tag{A2} \\
 &= \frac{1}{2} \left[\|\dot{\mathbf{X}}_j - \Theta(\mathbf{X})\Xi_j\|_{\mathbf{V}_{\epsilon_j}^{-1}}^2 + \|\Xi_j\|_{\mathbf{V}_{\Xi_j}^{-1}}^2 - \|\dot{\mathbf{X}}_j\|_{\hat{\Omega}_j^{-1}}^2 \right] \\
 &\quad + \frac{1}{2} \ln \det(\mathbf{V}_{\epsilon_j}) + \frac{1}{2} \ln \det(\mathbf{V}_{\Xi_j}) - \frac{1}{2} \ln \det(\Theta \mathbf{V}_{\Xi_j} \Theta^\top + \mathbf{V}_{\epsilon_j}) \\
 &\quad + (m + \frac{c}{2}) \ln(2\pi)
 \end{aligned}$$

For constant m , c , \mathbf{V}_{ϵ_j} and \mathbf{V}_{Ξ_j} , dependent variable data $\dot{\mathbf{X}}_j$ and alphabet Θ , (A2) reduces to the argument of (16).

Now consider isotropic variances for the noise $\mathbf{V}_{\epsilon_j} = \sigma_{\epsilon_j}^2 \mathbf{I}_m$ and prior $\mathbf{V}_{\Xi_j} = \sigma_{\Xi_j}^2 \mathbf{I}_c$, where \mathbf{I}_s is the identity matrix of size s , then $\mathbf{V}_{\epsilon_j}^{-1} = \mathbf{I}_m / \sigma_{\epsilon_j}^2$, $\mathbf{V}_{\Xi_j}^{-1} = \mathbf{I}_c / \sigma_{\Xi_j}^2$, $\det(\mathbf{V}_{\epsilon_j}) = \sigma_{\epsilon_j}^{2m}$, $\det(\mathbf{V}_{\Xi_j}) = \sigma_{\Xi_j}^{2c}$ and $\hat{\Omega}_j = \sigma_{\Xi_j}^2 \Theta \Theta^\top + \sigma_{\epsilon_j}^2 \mathbf{I}_m$. The objective function (A2) becomes:

$$\begin{aligned}
 J^B(\Xi_j) &= \frac{1}{2} \left[\frac{1}{\sigma_{\epsilon_j}^2} \|\dot{\mathbf{X}}_j - \Theta(\mathbf{X})\Xi_j\|_2^2 + \frac{1}{\sigma_{\Xi_j}^2} \|\Xi_j\|_2^2 - \|\dot{\mathbf{X}}_j\|_{\hat{\Omega}_j^{-1}}^2 \right] \\
 &\quad + m \ln \sigma_{\epsilon_j} + c \ln \sigma_{\Xi_j} - \frac{1}{2} \ln \det(\sigma_{\Xi_j}^2 \Theta \Theta^\top + \sigma_{\epsilon_j}^2 \mathbf{I}_m) \tag{A3} \\
 &\quad + (m + \frac{c}{2}) \ln(2\pi)
 \end{aligned}$$

For constant m , c , σ_{ϵ_j} and σ_{Ξ_j} , dependent variable data $\dot{\mathbf{X}}_j$ and alphabet Θ , the minimization problem reduces to^{26,41,42,52}:

$$\begin{aligned}
 \hat{\Xi}_j^{\text{reg}2} &= \arg \min_{\Xi_j} J(\Xi_j) \tag{A4} \\
 J^{\text{reg}2}(\Xi_j) &= \|\dot{\mathbf{X}}_j - \Theta(\mathbf{X})\Xi_j\|_2^2 + \kappa_j \|\Xi_j\|_2^2
 \end{aligned}$$

which we identify as Tikhonov regularization with residual term $\|\dot{\mathbf{X}}_j - \Theta(\mathbf{X})\Xi_j\|_2^2$, regularization term $\|\Xi_j\|_2^2$ and regularization coefficient $\kappa_j = \sigma_{\epsilon_j}^2 / \sigma_{\Xi_j}^2$.

The AIC and BIC metrics (33) can also be interpreted⁵² as crude approximations of (A2) or (A3). However, since the regularization term (hence the prior) is absent, these provide metrics for a modified maximum likelihood method rather than for Bayesian inference.

REFERENCES

- ¹S.L. Brunton, J.L. Proctor & J.N. Kutz, “Discovering governing equations from data by sparse identification of nonlinear dynamical systems”, *PNAS* **113**(15), 3932-3937 (2016).
- ²H. Schaeffer, “Learning partial differential equations via data discovery and sparse optimization”, *Proc. R. Soc. A* **473**, 20160446 (2016).
- ³S.H. Rudy, S.L. Brunton, J.L. Proctor & J.N. Kutz, “Data-driven discovery of partial differential equations”, *Sci. Adv.* **3**, e1602614 (2017).
- ⁴N.M. Mangan, J.N. Kutz, S.L. Brunton & J.L. Proctor, “Model selection for dynamical systems via sparse regression and information criteria”, *Roy Soc Proc A* **473**, 20170009 (2017).
- ⁵E. Kaiser, J.N. Kutz & S.L. Brunton, “Sparse identification of nonlinear dynamics for model predictive control in the low-data limit”, *Proc. R. Soc. A* **474**, 20180335 (2018).
- ⁶M. Quade, M. Abel, J.N. Kutz & S.L. Brunton, “Sparse identification of nonlinear dynamics for rapid model recovery”, *Chaos* **28**, 063116 (2018).
- ⁷N.M. Mangan, T. Askham, S.L. Brunton, J.N. Kutz & J.L. Proctor, “Model selection for hybrid dynamical systems via sparse regression”, *Proc. R. Soc. A* **475**, 20180534 (2019).
- ⁸K. Champion, B. Lusch, J.N. Kutz & S.L. Brunton, “Data-driven discovery of coordinates and governing equations”, *PNAS* **116**(45), 22445-22451 (2019).
- ⁹K. Champion, P. Zheng, A.Y. Aravkin, S.L. Brunton & J.N. Kutz, “A unified sparse optimization framework to learn parsimonious physics-informed models from data”, *IEEE Access* **8**, 169259-169271 (2020).
- ¹⁰K. Kaheman, J.N. Kutz & S.L. Brunton, “SINDy-PI: a robust algorithm for parallel implicit sparse identification of nonlinear dynamics”, *Proc. R. Soc. A* **476**, 20200279 (2020).
- ¹¹U. Fasel, J.N. Kutz, B.W. Brunton & S.L. Brunton “Ensemble-SINDy: Robust sparse model discovery in the low-data, high-noise limit, with active learning and control”, *Proc. R. Soc. A* **478**, 20210904 (2022).
- ¹²T. Bayes, T. (presented by R. Price), “An essay towards solving a problem in the doctrine of chance”, *Phil. Trans. Royal Soc. London* **53**, 370-418 (1763).
- ¹³P. Laplace, “Mémoire sur la probabilité des causes par les évènements”, *l’Académie Royale des Sciences*, **6**, 621-656 (1774).
- ¹⁴E.T. Jaynes (G.L. Bretthorst, ed.), *Probability Theory: The Logic of Science* (Cambridge

- Univ. Press, Cambridge, UK, 2003).
- ¹⁵U. von Toussaint, “Bayesian inference in physics”, *Rev. Mod. Phys.* **83**(3), 943-999 (2011).
- ¹⁶G. Polya, *Mathematics and Plausible Reasoning, Vol II, Patterns of Plausible Inference*, (Princeton Univ. Press, Princeton, NJ, USA, 1954).
- ¹⁷R.T. Cox, *The Algebra of Probable Inference* (John Hopkins Press, Baltimore, MD, USA, 1961).
- ¹⁸J. Venn, *The Logic of Chance* (Macmillan & Co, London, UK, 1888).
- ¹⁹R.A. Fisher, *Statistical Methods for Research Workers* (Oliver and Boyd, Edinburgh, UK, 1925).
- ²⁰J. Neyman & E.S. Pearson, “On the problem of the most efficient tests of statistical hypotheses”, *Phil. Trans. R. Soc. Lond. A* **231**(694-706), 289-337 (1933).
- ²¹W. Feller, *An Introduction to Probability Theory and Its Applications*, Volume II (John Wiley and Sons, Inc., NY, USA, 1966).
- ²²A. Mohammad-Djafari, “Inverse problems in signal and image processing and Bayesian inference framework: from basic to advanced Bayesian computation”, Scube seminar, L2S, CentraleSupélec, Gif-sur-Yvette, France (2015).
- ²³A. Mohammad-Djafari. & M. Dumitru, “Bayesian sparse solutions to linear inverse problems with non-stationary noise with Student-t priors”, *Digital Signal Proc.* **47**, 128-156 (2015).
- ²⁴A. Mohammad-Djafari, “Approximate Bayesian computation for big data”, Tutorial, MaxEnt 2016, July 10-15, 2016, Ghent, Belgium (2016).
- ²⁵A. Teckentrup, “Introduction to the Bayesian approach to inverse problems”, presentation, MaxEnt 2018, July 6, 2018, London, UK (2018).
- ²⁶D. Calvetti & E. Somersalo, “Inverse problems: From regularization to Bayesian inference”, *Wiley Interdisc. Rev.: Comp. Stat.* **10**(2), e1427 (2018).
- ²⁷W. Pan, Y. Yuan, J. Goncalves & G.-B. Stan, “A sparse Bayesian approach to the identification of nonlinear state- space systems”, *IEEE Trans. Automatic Control*, **61**(1), 182-187 (2016).
- ²⁸S. Zhang & G. Lin, “Robust data-driven discovery of governing physical laws with error bars”, *Proc. Royal Society A: Math. Phys. Eng. Sci.*, **474**(2217), 20180305 (2018).
- ²⁹R.K. Niven, A. Mohammad-Djafari, L. Cordier, M. Abel & M. Quade, “Bayesian identification of dynamical systems”, *MDPI Proc.* **33**(1), 33 (2019).

- ³⁰A. Chiuso & G. Pillonetto, “System identification: a machine learning perspective”, *Annual Review of Control, Robotics, and Autonomous Systems* **2**, 281-304 (2019).
- ³¹A. Chen & G. Lin, “Robust data-driven discovery of partial differential equations with time-dependent coefficients”, *arXiv:2102.01432v1*.
- ³²N. Taghavi, *Developing a Geospatial Bayesian Probabilistic Method for Groundwater Vulnerability Assessment*, PhD Thesis, The University of New South Wales, Canberra, ACT, Australia (unpub.) (2024).
- ³³Y. Yuan, X. Li, L. Li, F.J. Jiang, X. Tang, F. Zhang, J. Goncalves, H.U. Voss, H. Ding & J. Kurths, “Machine discovery of partial differential equations from spatiotemporal data: A sparse Bayesian learning framework”, *Chaos* **33**, 113122 (2023).
- ³⁴S. Roberts, M. Osborne, M. Ebden, S. Reece, N. Gibson & S. Aigrain, “Gaussian processes for time-series modelling”, *Phil. Trans. R. Soc. A* **371**, 20110550 (2013).
- ³⁵A. Svensson & T.B. Schön, “A flexible state-space model for learning nonlinear dynamical systems”, *Automatica* **80**, 189-199 (2017).
- ³⁶M. Raissi & G.E. Karniadakis, “Hidden physics models: Machine learning of nonlinear partial differential equations”, *J. Comp. Phys.* **357**,125-141 (2018).
- ³⁷A.L. Teckentrup, “Convergence of Gaussian process regression with estimated hyperparameters and applications in Bayesian inverse problems”, *SIAM/ASA J. Unc. Quant.* **8**(4), 1310-1337 (2020).
- ³⁸S.M. Hirsh, D.A. Barajas-Solano & J.N. Kutz, “Sparsifying priors for Bayesian uncertainty quantification in model discovery”, *R. Soc. Open Sci.* **9**, 211823 (2022).
- ³⁹A. Rinkens, C.V. Verhoosel & N.O. Jaensson, “Uncertainty quantification for the squeeze flow of generalized Newtonian fluids”, *J. Non-Newtonian Fluid Mech.*, **322**, 105154 (2023).
- ⁴⁰A. Kontogiannis, S.V. Elgersma, A.J. Sederman & M.P. Juniper, “Joint reconstruction and segmentation of noisy velocity images as an inverse Navier–Stokes problem”, *J. Fluid Mech.* **944**, A40 (2022).
- ⁴¹R.C. Aster, B. Borchers & C.H. Thurber, *Parameter Estimation and Inverse Problems*, 2nd ed. (Elsevier, Amsterdam, Netherlands, 2013).
- ⁴²J.M. Bardsley, *Computational Uncertainty Quantification for Inverse Problems* (SIAM, Philadelphia, PA, USA, 2018).
- ⁴³A.N. Tikhonov, “Solution of incorrectly formulated problems and the regularization method”, *Doklady Akademii Nauk SSSR* **151**, 501-504 (1963).

- ⁴⁴A.E. Hoerl & R.W. Kennard, “Ridge regression: Biased estimation for nonorthogonal problems”, *Technometrics* **12**(1), 55–67 (1970).
- ⁴⁵F. Santosa & W.W. Symes, “Linear inversion of band-limited reflection seismograms”, *SIAM J. Sci. Stat. Comp.* **7**(4), 1307-1330 (1986).
- ⁴⁶R. Tibshirani, “Regression shrinkage and selection via the Lasso”, *J Royal Stat. Soc. B* **58**(1), 267-288 (1996).
- ⁴⁷S.L. Brunton, B.W. Brunton, J.L. Proctor, E. Kaiser & J.N. Kutz, “Koopman invariant subspaces and finite linear representations of nonlinear dynamical systems for control”, *PLOS One*, **11**(2), e0150171 (2016).
- ⁴⁸S.L. Brunton, B.W. Brunton, J.L. Proctor, E. Kaiser & J.N. Kutz, “Chaos as an intermittently forced linear system”, *Nature Comm* **8**, 1 (2017).
- ⁴⁹K. Taira, S.L. Brunton, S.T.M. Dawson, C.W. Rowley, T. Colonius, B.J. McKeon, O.T. Schmidt, S. Gordeyev, V. Theofilis & L.S. Ukeiley, “Modal analysis of fluid flows: an overview”, *AIAA Journal* **55**(12), 4013-4041 (2017).
- ⁵⁰L. Zhang & H. Schaeffer, “On the convergence of the SINDy algorithm”, *Multiscale Model. Simul.* **17**(3), 948-972 (2019).
- ⁵¹A. Tarantola, *Inverse Problem Theory and Methods for Model Parameter Estimation* (SIAM, Philadelphia, PA, USA, 2005).
- ⁵²C.M. Bishop, *Pattern Recognition and Machine Learning* (Springer, MY, USA, 2006).
- ⁵³P.D. Hoff, *A First Course in Bayesian Statistical Methods* (Springer, Dordrecht, Germany, 2009).
- ⁵⁴L. Tenorio, *An Introduction to Data Analysis and Uncertainty Quantification for Inverse Problems* (SIAM, Philadelphia, PA, USA, 2017).
- ⁵⁵R. Bontekoe, *What is Your Model?: A Bayesian Tutorial* (Bontekoe Research, Amsterdam, Netherlands, 2023).
- ⁵⁶J. Skilling, “Nested Sampling”, *AIP Conf. Proc.* **735**, 395-405 (2004).
- ⁵⁷J.-M. Marin & C. Robert, *Bayesian Core: A Practical Approach to Computational Bayesian Statistics* (Springer, New York, NY, USA, 2007).
- ⁵⁸M. Clyde, M. Çetinkaya-Rundel, C. Rundel, D. Banks, C. Chai & L. Huang, *An Introduction to Bayesian Thinking. A Companion to the Statistics with R Course*, https://statswithr.github.io/book/_main.pdf, retrieved Dec 2023.
- ⁵⁹K. Burnham & D. Anderson, *Model selection and multi-model inference*, 2nd ed. (Springer,

Berlin, Germany, 2002).

- ⁶⁰E.N. Lorenz, “Deterministic nonperiodic flow”, *J. Atmos. Sci.* **20**(2), 130-141 (1963).
- ⁶¹S. Lynch, *Dynamical Systems with Applications using MATLAB* (BirkhäuserBoston, Springer, New York, NY, USA, 2004).
- ⁶²R.R. Vance, “Predation and resource partitioning in one predator-two prey model community”, *The American Naturalist*, **112**, 797-813 (1978).
- ⁶³M.E. Gilpin, “Spiral chaos in a predator-prey model”, *The American Naturalist* **113**(2), 306-308 (1979).
- ⁶⁴A.L. Shil’nikov, L.P. Shil’nikov & D.V. Turaev, “Normal forms and Lorenz attractors”, *Int. J. Bifurc. Chaos* **3**(5), 1123-1139 (1993).
- ⁶⁵D. Lin, “Safe computation of logarithm-determinant of large matrix”, MATLAB Central File Exchange, <https://www.mathworks.com/matlabcentral/fileexchange/22026-safe-computation-of-logarithm-determinat-of-large-matrix>, retrieved January 19, 2024.
- ⁶⁶J. Pearl, *Probabilistic Reasoning in Intelligent Systems: Networks of Plausible Inference* (Morgan Kaufmann, San Francisco, CA, USA, 1988).
- ⁶⁷I. Psorakis, S. Roberts, M. Ebdon & B. Sheldon, “Overlapping community detection using Bayesian non-negative matrix factorization”, *Phys. Rev. E* **83**(6-2), 066114 (2011).

SUPPLEMENTARY INFORMATION

The supplementary information, given in Figures S1-S17, provides a more complete set of figures for the case studies examined in the manuscript.

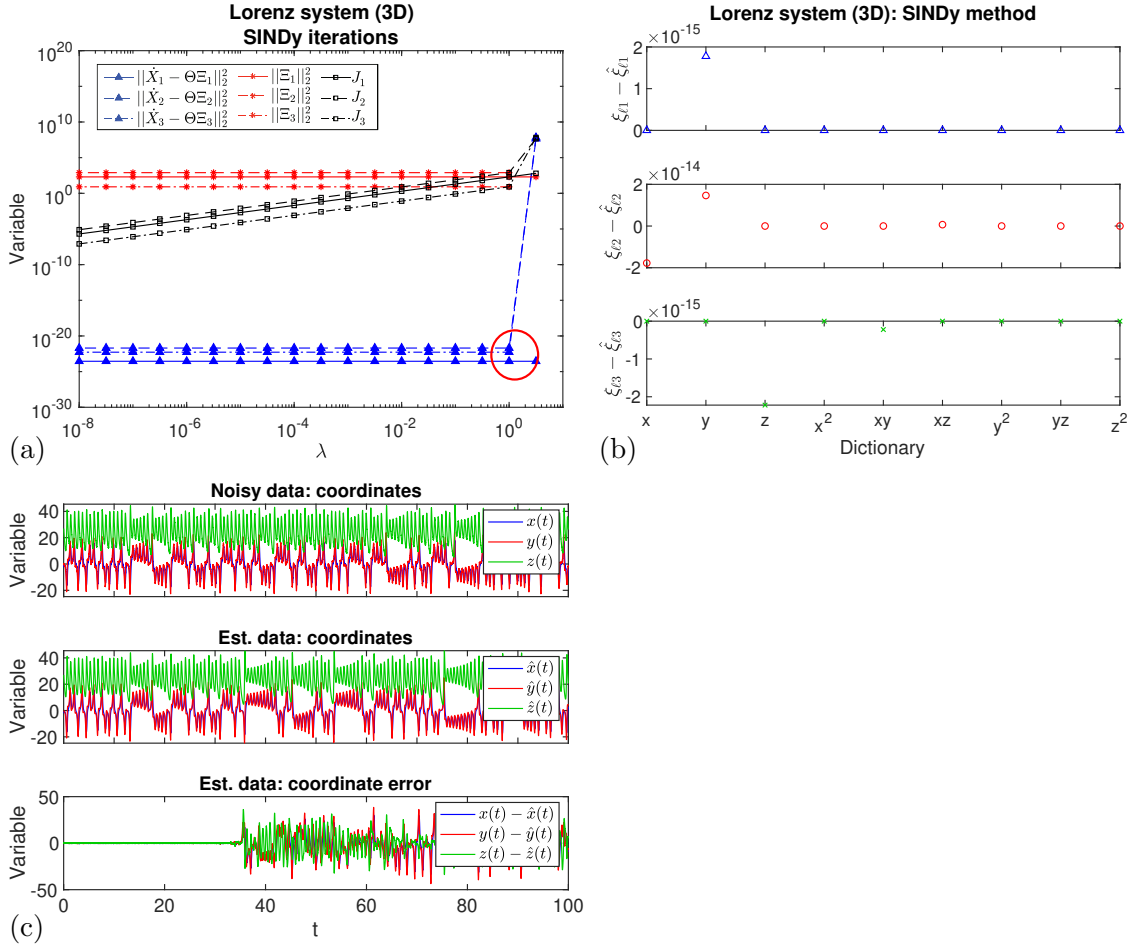


FIG. S1. Lorenz second-order polynomial regularization using SINDy, $t = 100$, $t_{step} = 0.01$, $\varepsilon = 0.2$: (a) plots of 2-norm residual, regularization and objective functions (7) with decreasing λ , showing the optimal iteration ($k = 3$); (b) optimal error in predicted coefficients $\xi_{ij} - \hat{\xi}_{ij}$; and (c) original and optimal predicted data and their differences.

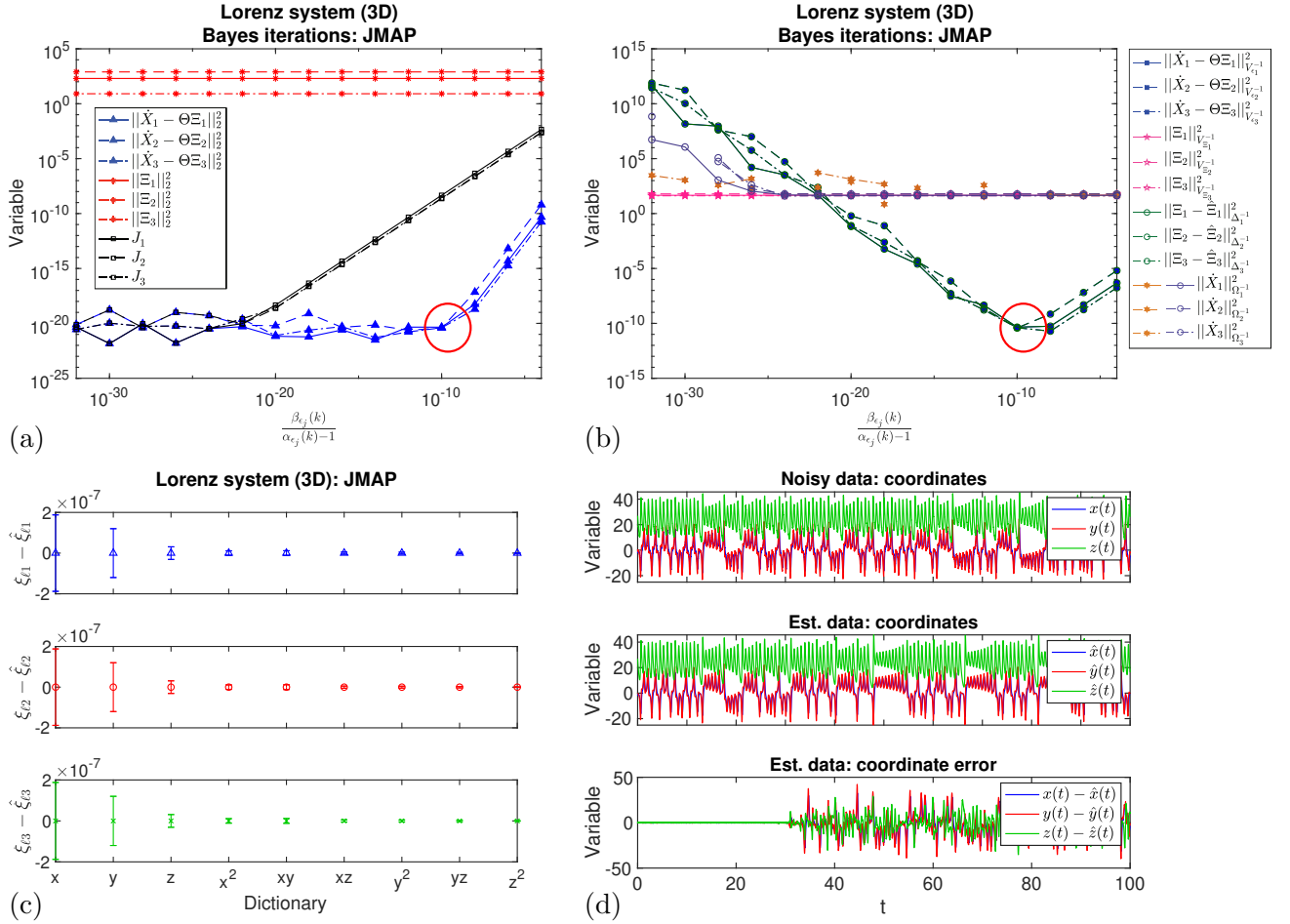


FIG. S2. Lorenz second-order polynomial regularization using JMAP, $t = 100$, $t_{step} = 0.01$, $\epsilon = 0.2$, showing the iteration sequence with decreasing $E_{\epsilon_{ij}}$, including (a) 2-norm residual, regularization and objective functions (7), showing the optimal iteration ($k = 5$); (b) Gaussian norms for the prior, likelihood, posterior and evidence, showing the optimal iteration ($k = 5$); (c) optimal error in predicted coefficients $\xi_{ij} - \hat{\xi}_{ij}$, with error bars from the posterior covariance (18); and (d) original and optimal predicted data and their differences.

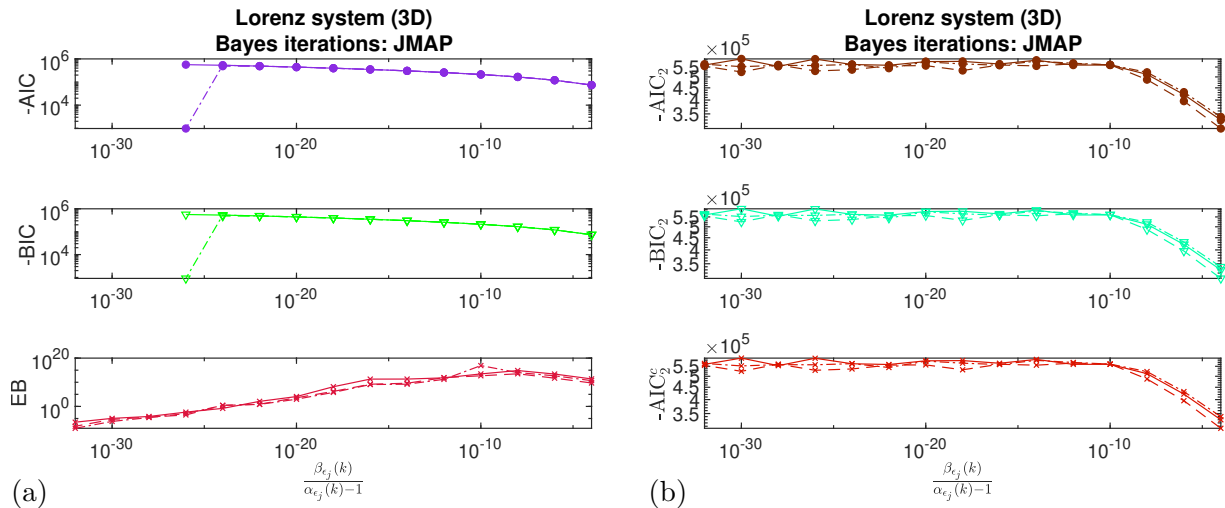


FIG. S3. Lorenz second-order polynomial regularization using JMAP, $t = 100$, $t_{step} = 0.01$, $\varepsilon = 0.2$, showing the alternative metrics by iteration sequence: (a) AIC, BIC and EB (33)-(35), and (b) 2-norm approximations to AIC, BIC and AIC_C.

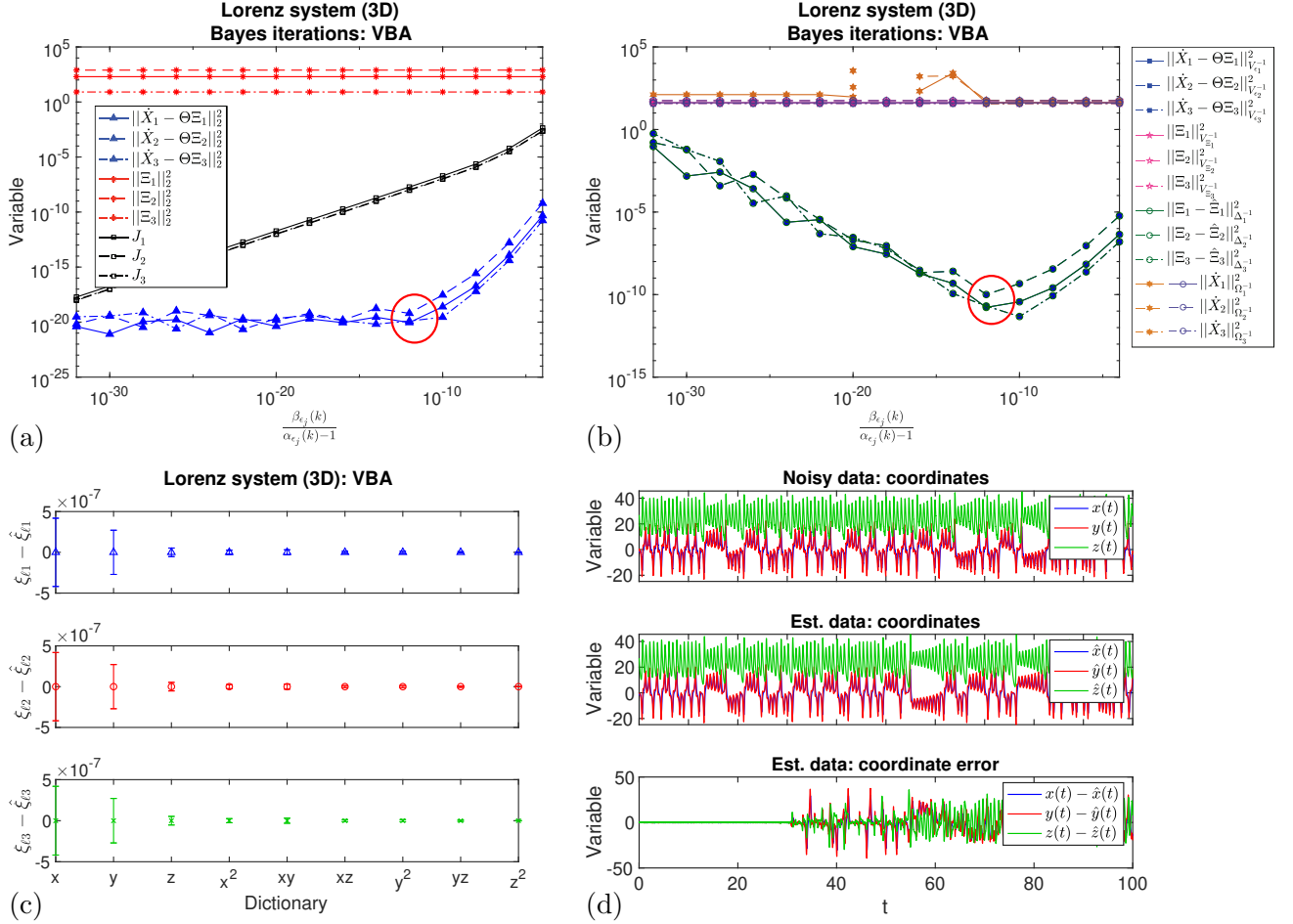


FIG. S4. Lorenz second-order polynomial regularization using VBA, $t = 100$, $t_{step} = 0.01$, $\epsilon = 0.2$, showing the iteration sequence with decreasing $E_{\epsilon_{ij}}$, including (a) 2-norm residual, regularization and objective functions (7), showing the optimal iteration ($k = 6$); (b) Gaussian norms for the prior, likelihood, posterior and evidence, showing the optimal iteration ($k = 6$); (c) optimal error in predicted coefficients $\xi_{ij} - \hat{\xi}_{ij}$, with error bars from the posterior covariance (18); and (d) original and optimal predicted data and their differences.

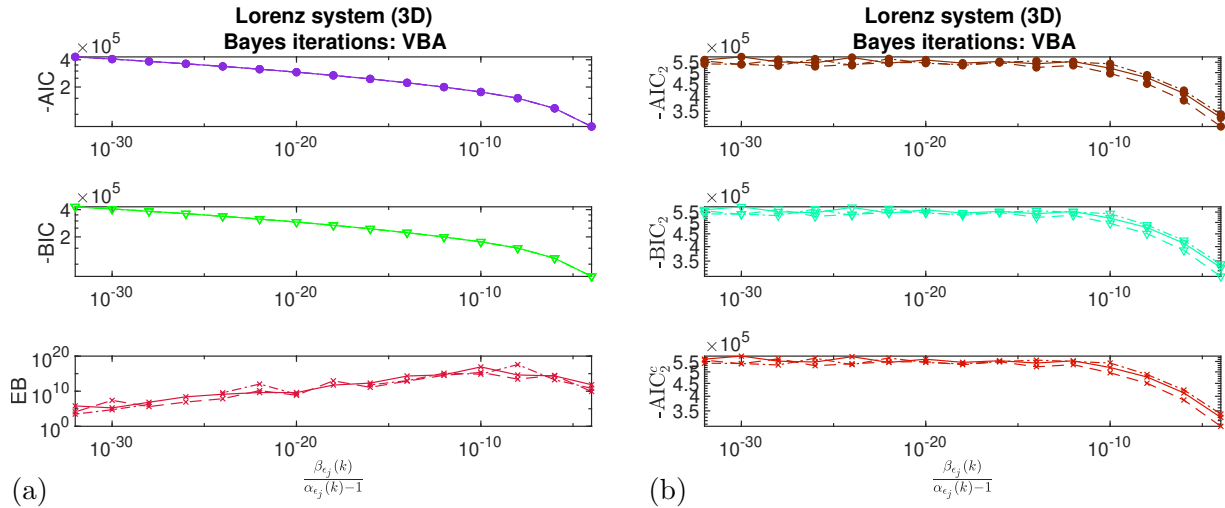


FIG. S5. Lorenz second-order polynomial regularization using VBA, $t = 100$, $t_{step} = 0.01$, $\varepsilon = 0.2$, showing the alternative metrics by iteration sequence: (a) AIC, BIC and EB (33)-(35), and (b) 2-norm approximations to AIC, BIC and AIC_c .

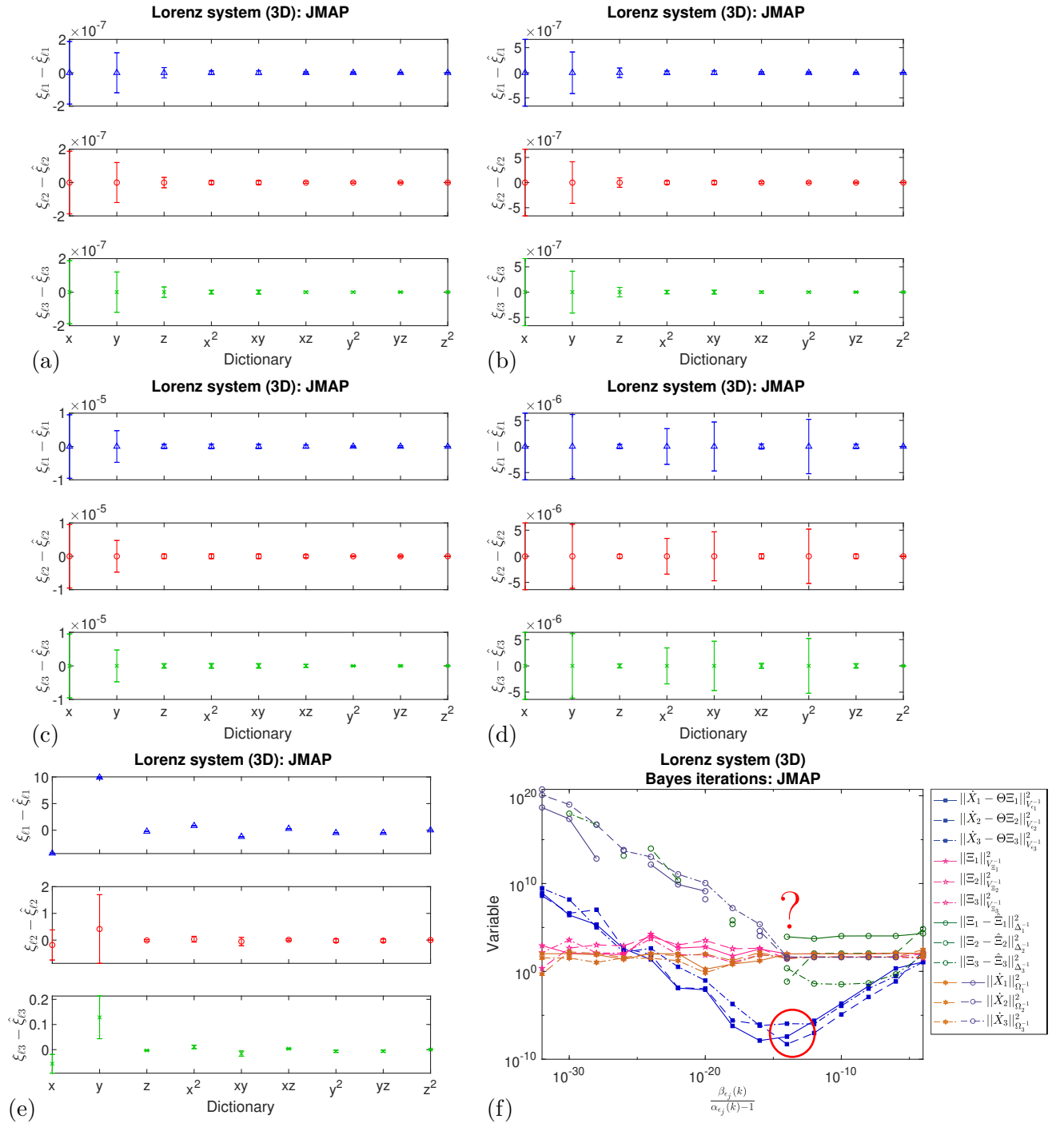


FIG. S6. Lorenz system, effect of time-series length on JMAP regularization for $t_{step} = 0.01$, $\varepsilon = 0.2$: (a) $t = 100$; (b) $t = 10$; (c) $t = 1$; (d) $t = 0.1$; and (e) $t = 0.08$; (f) Gaussian norms for the prior, likelihood, posterior and evidence for $t = 0.08$, $t_{step} = 0.01$, $\varepsilon = 0.2$, showing breakdown of the JMAP algorithm for this small number of points ($m = 8$).

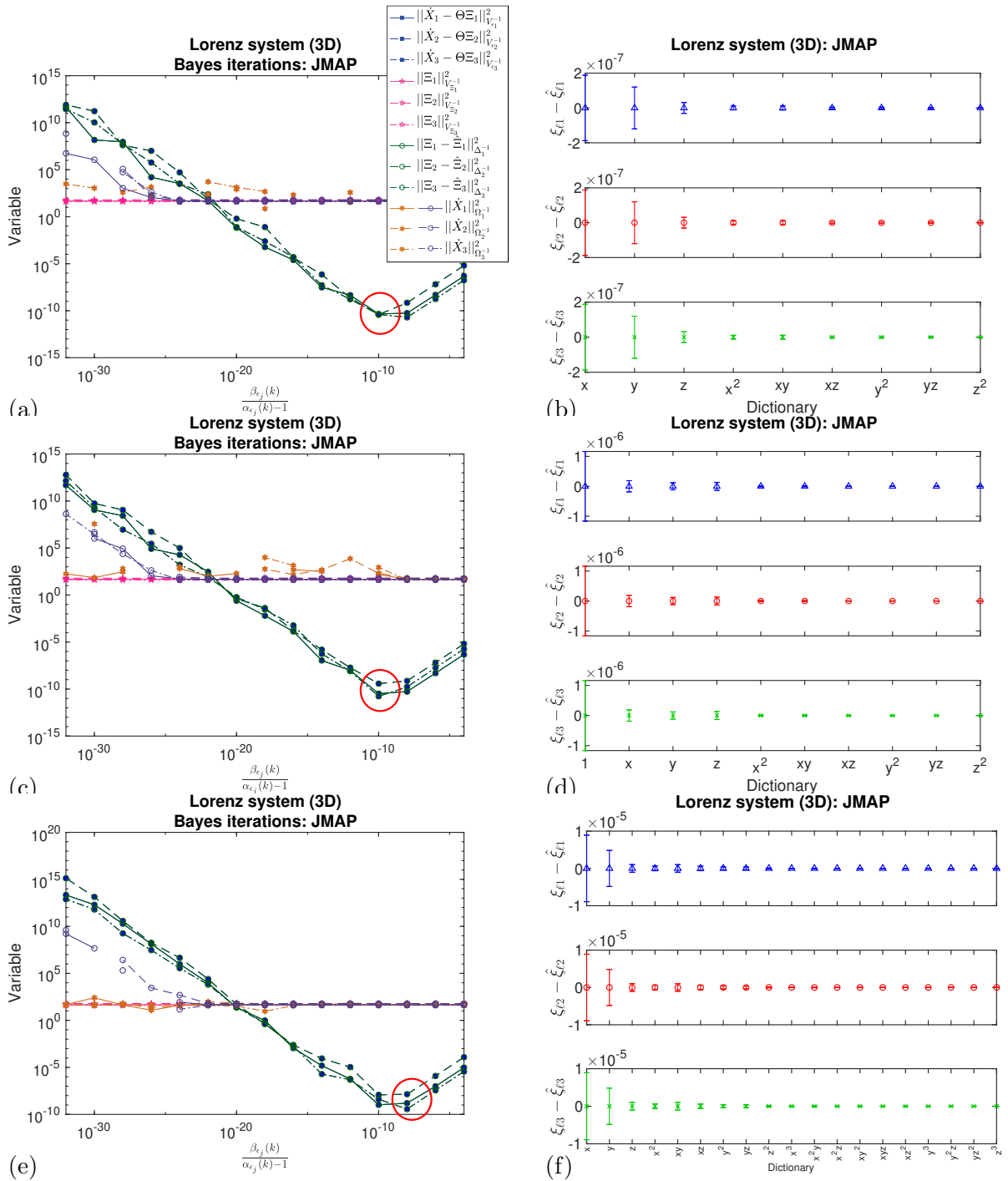


FIG. S7. Lorenz system, effect of different alphabets on JMAP regularization for $t = 100$, $t_{step} = 0.01$, $\varepsilon = 0.2$ with (a)-(b) polynomials to second order, (c)-(d) polynomials to second order with a column of 1s, and (e)-(f) polynomials to third order; (a),(c),(e) Gaussian norms for the prior, likelihood, posterior and evidence, with the optimal iteration; and (b),(d),(f) optimal error in predicted coefficients $\xi_{lj} - \hat{\xi}_{lj}$, with error bars calculated from the posterior covariance (18).

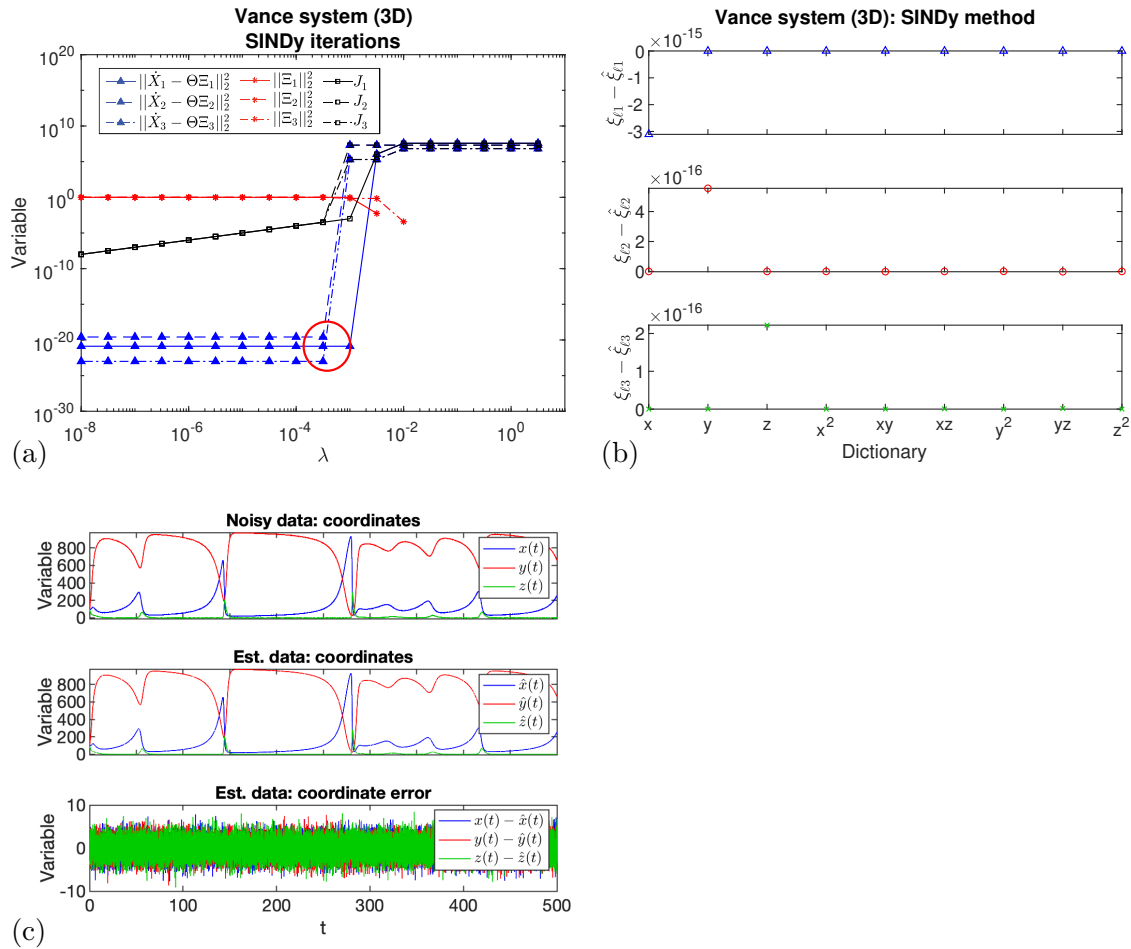


FIG. S8. Vance second-order polynomial regularization using SINDy, $t = 500$, $t_{step} = 0.02$, $\varepsilon = 2.0$: (a) plots of 2-norm residual, regularization and objective functions (7) with decreasing λ , showing the optimal iteration ($k = 10$); (b) optimal error in predicted coefficients $\xi_{ij} - \hat{\xi}_{ij}$; and (c) original and optimal predicted data and their differences.

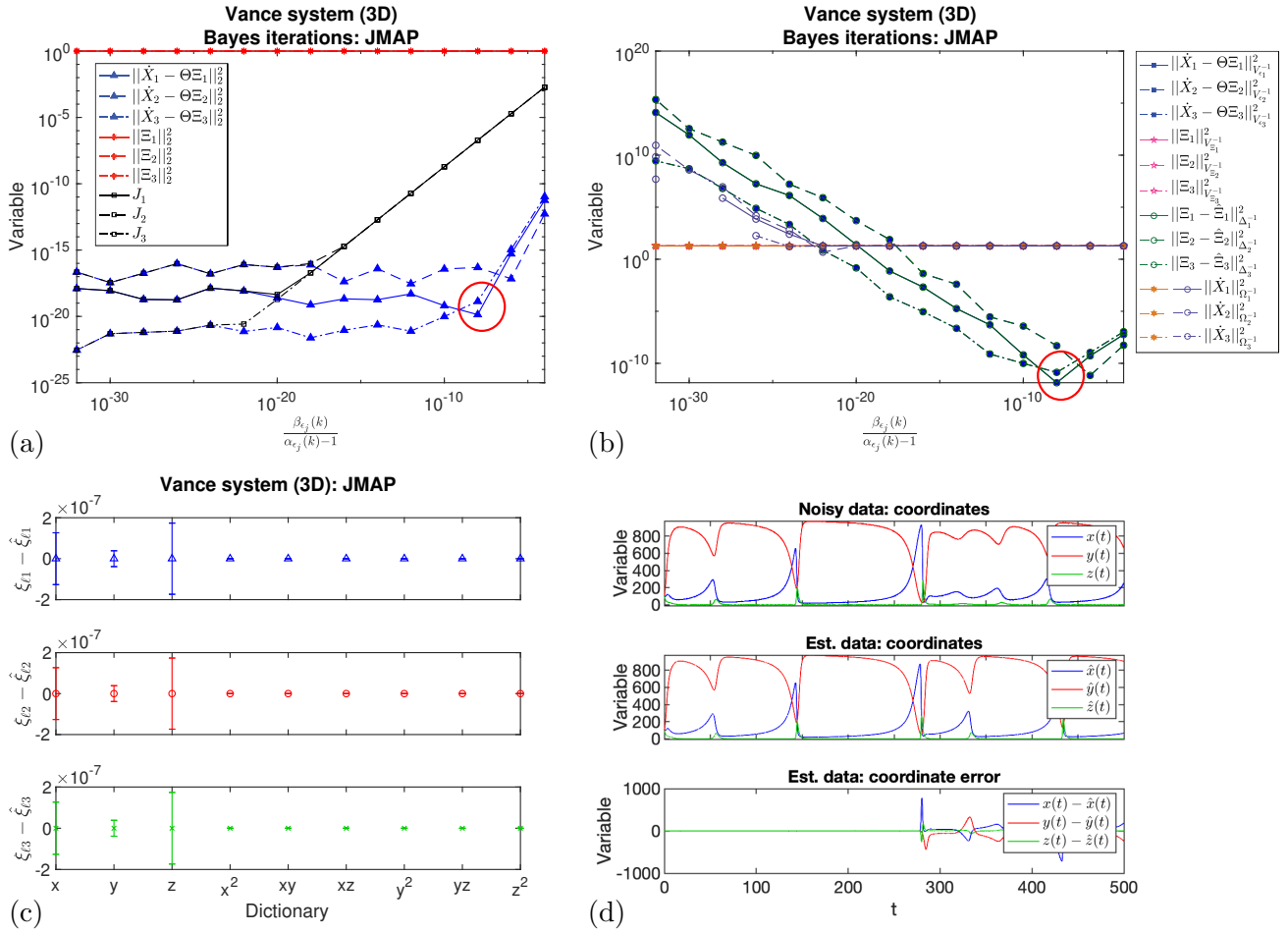


FIG. S9. Vance second-order polynomial regularization using JMAP, $t = 500$, $t_{step} = 0.02$, $\varepsilon = 2.0$, showing the iteration sequence with decreasing $E_{\varepsilon_{ij}}$, including (a) 2-norm residual, regularization and objective functions (7), showing the optimal iteration ($k = 4$); (b) Gaussian norms for the prior, likelihood, posterior and evidence, showing the optimal iteration ($k = 4$); (c) optimal error in predicted coefficients $\xi_{ij} - \hat{\xi}_{ij}$, with error bars from the posterior covariance (18); and (d) original and optimal predicted data and their differences.

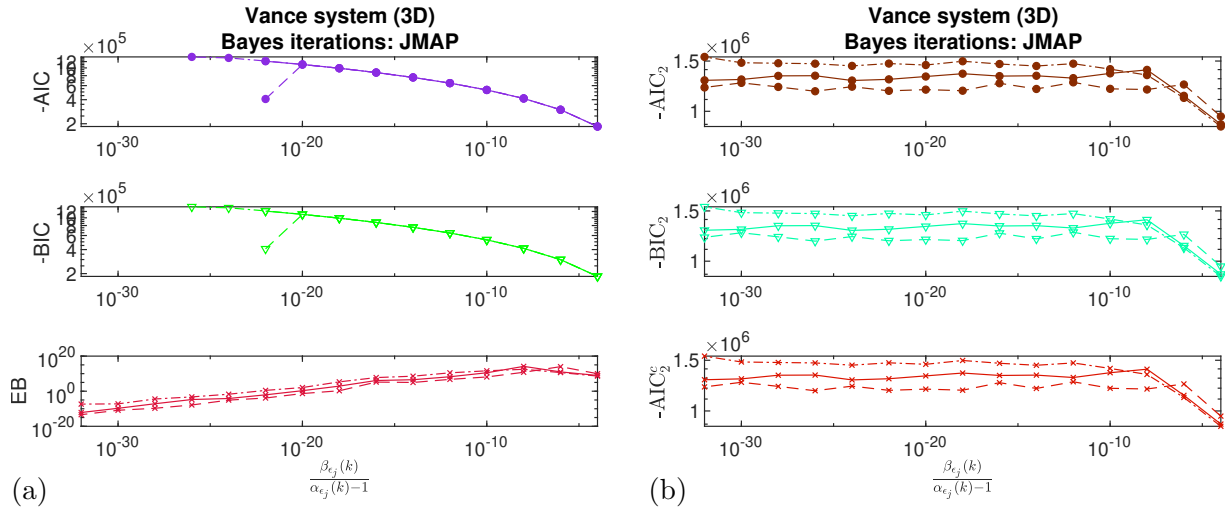


FIG. S10. Vance second-order polynomial regularization using JMAP, $t = 500$, $t_{step} = 0.02$, $\varepsilon = 2.0$, showing the alternative metrics by iteration sequence: (a) AIC, BIC and EB (33)-(35), and (b) 2-norm approximations to AIC, BIC and AIC_c .

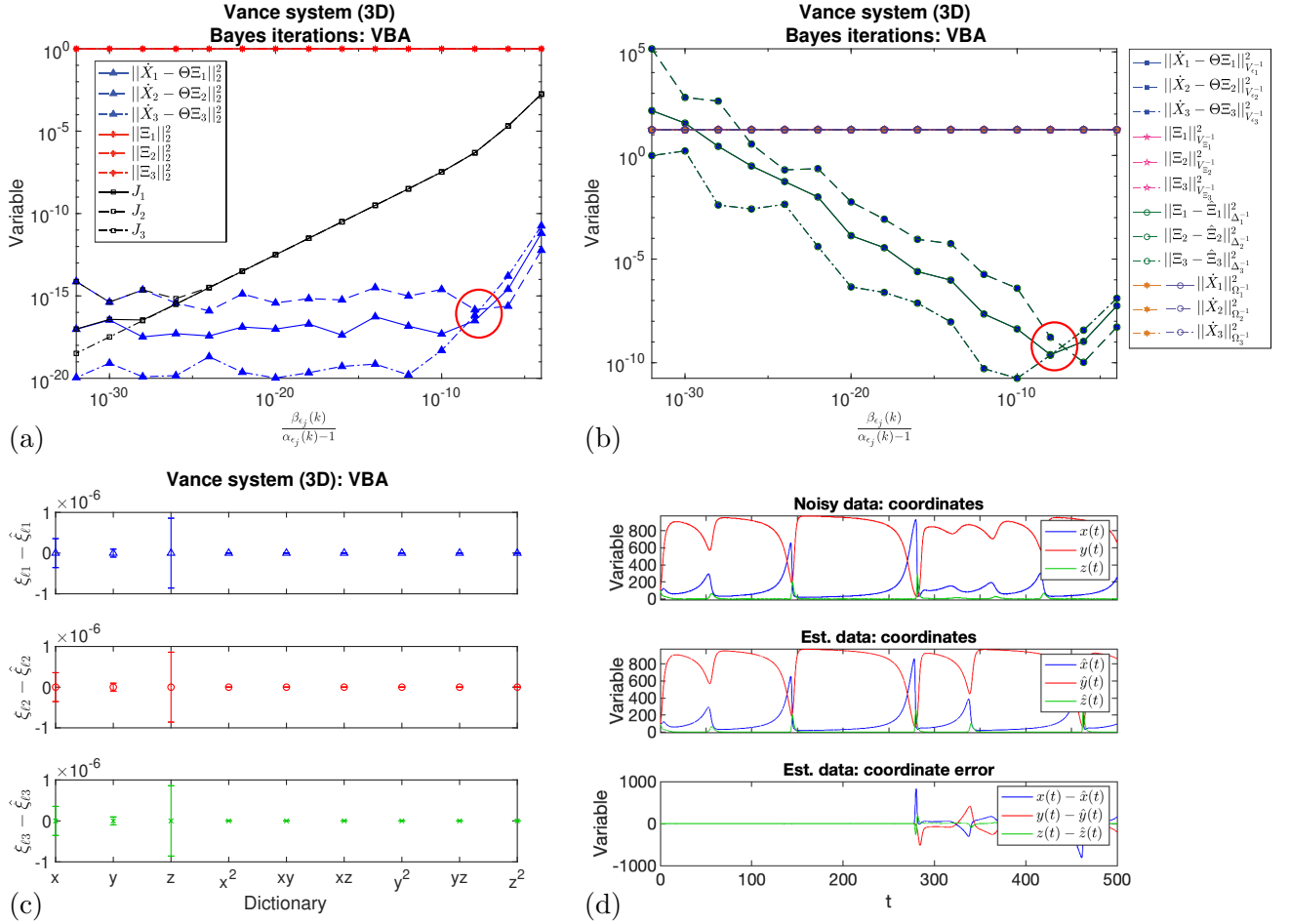


FIG. S11. Vance second-order polynomial regularization using VBA, $t = 500$, $t_{step} = 0.02$, $\varepsilon = 2.0$, showing the iteration sequence with decreasing $E_{\varepsilon_{ij}}$, including (a) 2-norm residual, regularization and objective functions (7), showing the optimal iteration ($k = 4$); (b) Gaussian norms for the prior, likelihood, posterior and evidence, showing the optimal iteration ($k = 4$); (c) optimal error in predicted coefficients $\xi_{ij} - \hat{\xi}_{ij}$, with error bars from the posterior covariance (18); and (d) original and optimal predicted data and their differences.

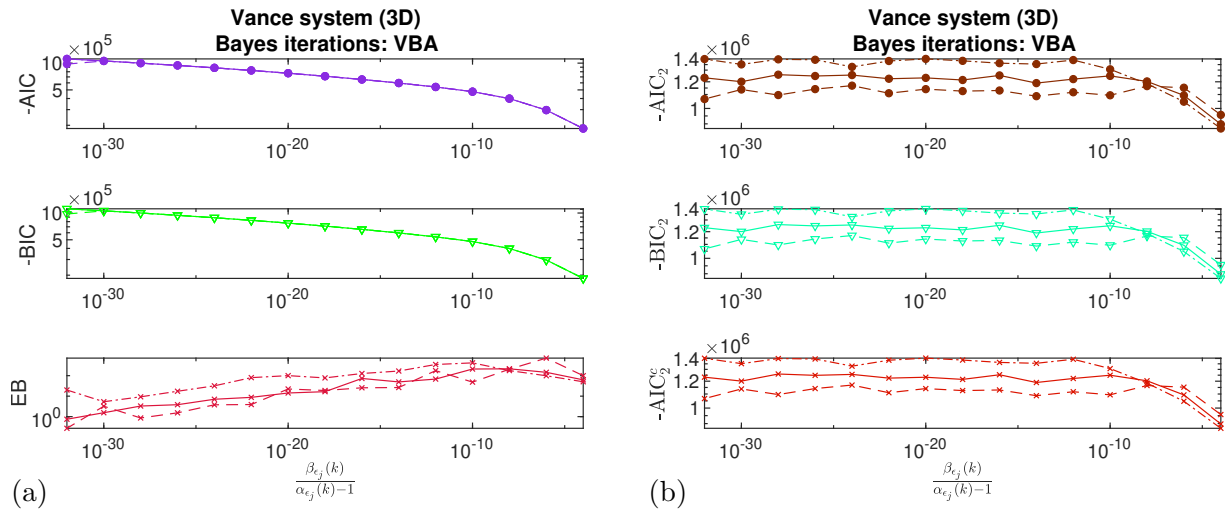


FIG. S12. Vance second-order polynomial regularization using VBA, $t = 500$, $t_{step} = 0.02$, $\varepsilon = 2.0$, showing the alternative metrics by iteration sequence: (a) AIC, BIC and EB (33)-(35), and (b) 2-norm approximations to AIC, BIC and AIC_C.

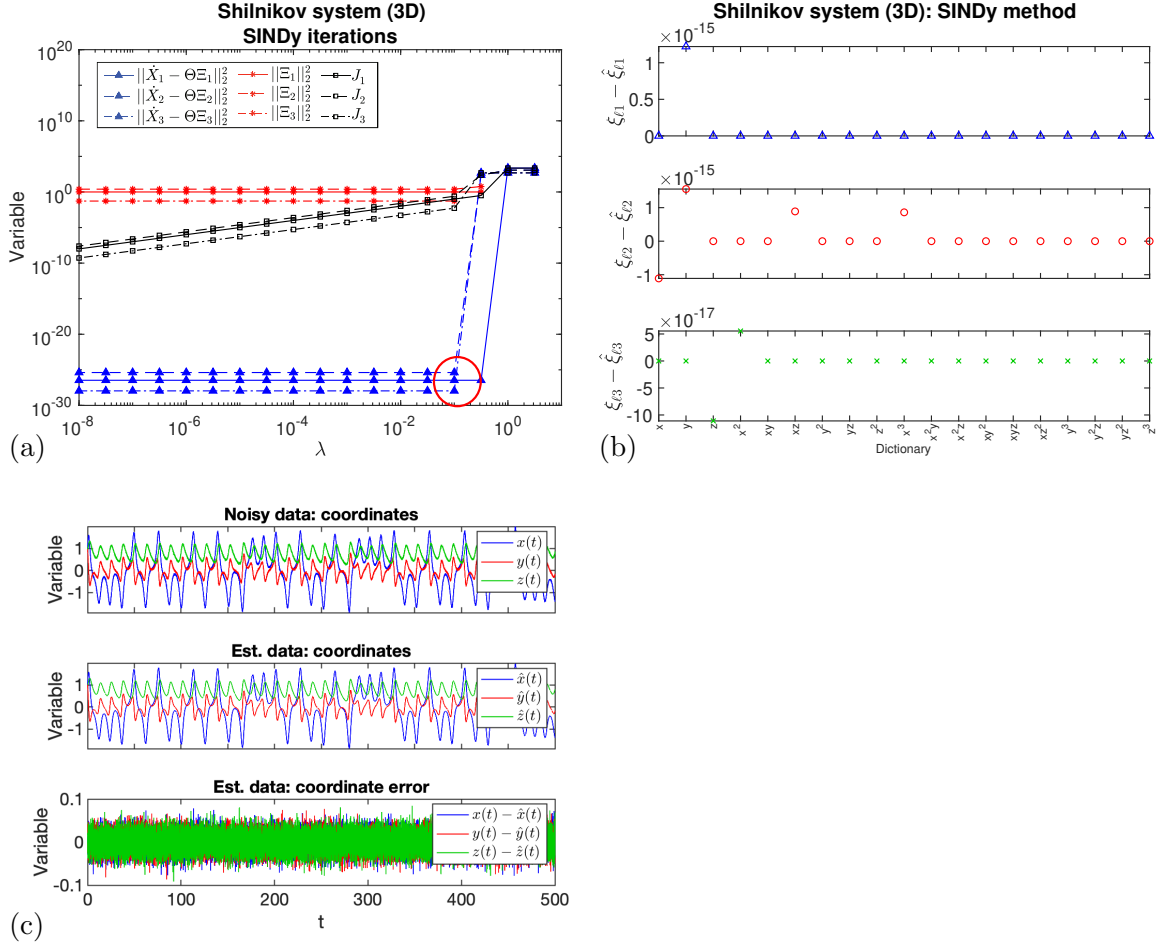


FIG. S13. Shilnikov third-order polynomial regularization using SINDy, $t = 500$, $t_{step} = 0.02$, $\varepsilon = 0.02$: (a) plots of 2-norm residual, regularization and objective functions (7) with decreasing λ , showing the optimal iteration ($k = 5$); (b) optimal error in predicted coefficients $\xi_{ij} - \hat{\xi}_{ij}$; and (c) original and optimal predicted data and their differences.

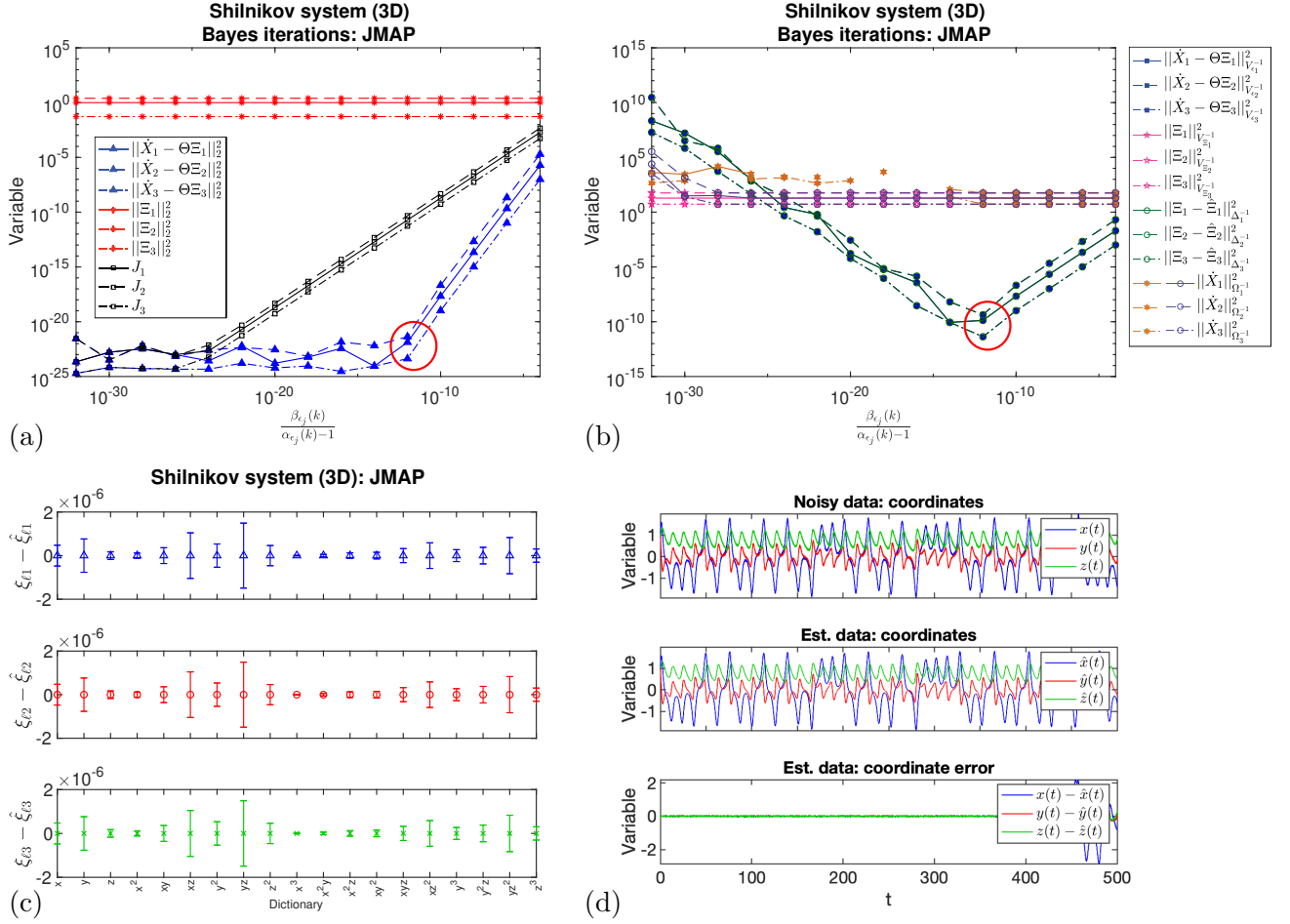


FIG. S14. Shilnikov third-order polynomial regularization using JMAP, $t = 500$, $t_{step} = 0.02$, $\varepsilon = 0.02$, showing the iteration sequence with decreasing $E_{\varepsilon_{ij}}$, including (a) 2-norm residual, regularization and objective functions (7), showing the optimal iteration ($k = 6$); (b) Gaussian norms for the prior, likelihood, posterior and evidence, showing the optimal iteration ($k = 6$); (c) optimal error in predicted coefficients $\xi_{ij} - \hat{\xi}_{ij}$, with error bars from the posterior covariance (18); and (d) original and optimal predicted data and their differences.

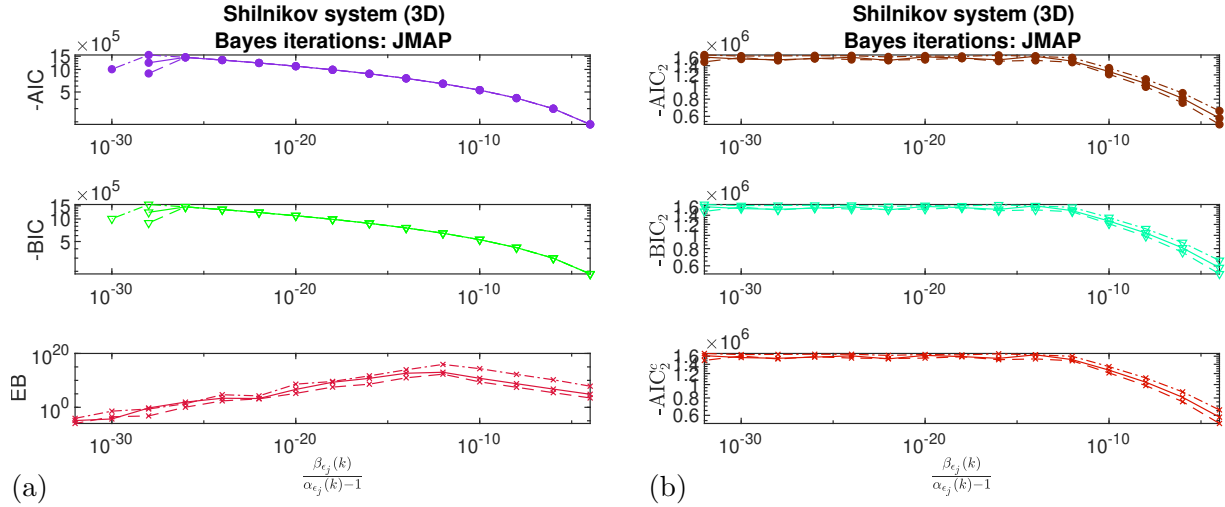


FIG. S15. Shilnikov third-order polynomial regularization using JMAP, $t = 500$, $t_{step} = 0.02$, $\varepsilon = 0.02$, showing the alternative metrics by iteration sequence: (a) AIC, BIC and EB (33)-(35), and (b) 2-norm approximations to AIC, BIC and AIC_c .

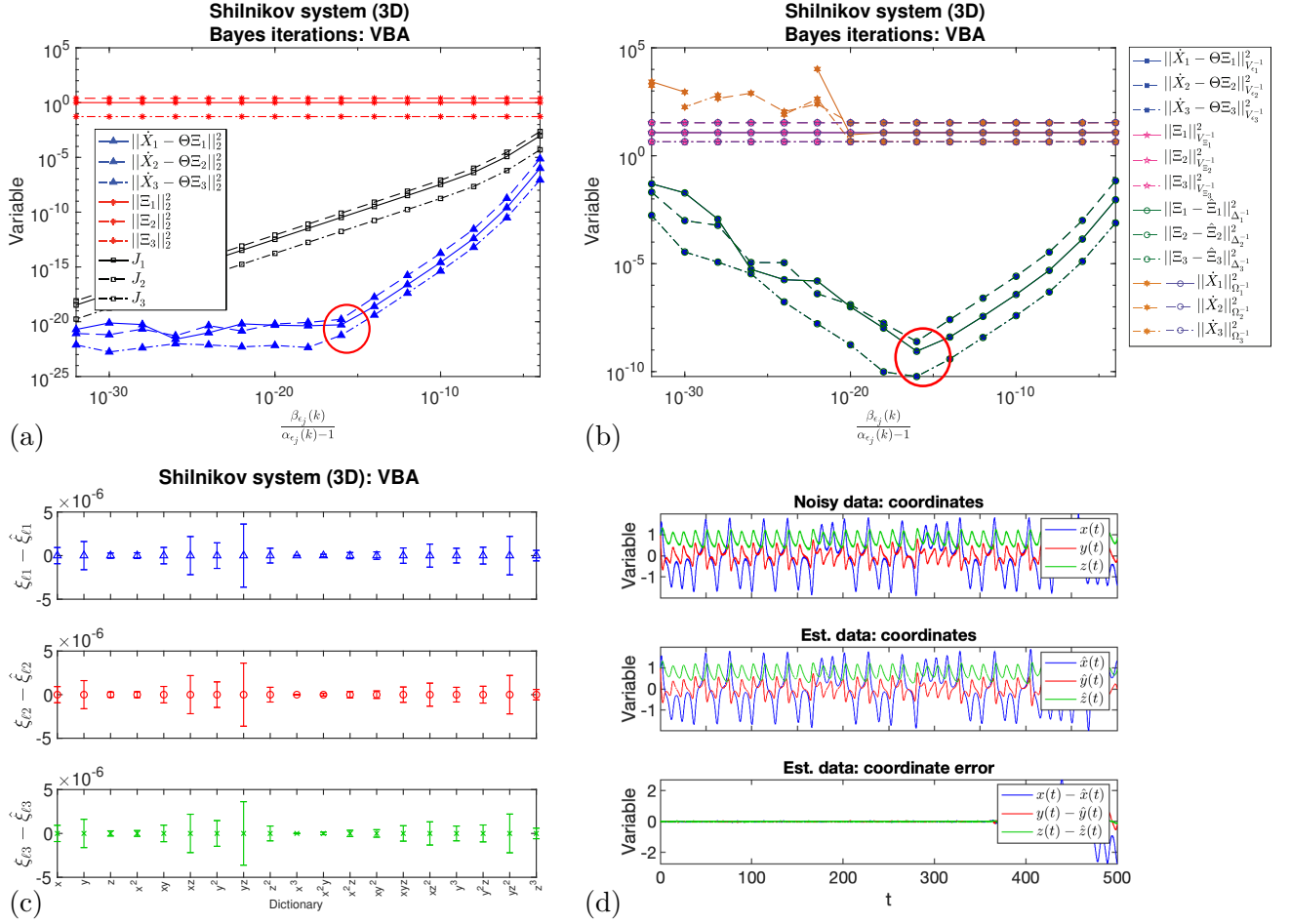


FIG. S16. Shilnikov third-order polynomial regularization using VBA, $t = 500$, $t_{step} = 0.02$, $\epsilon = 0.02$, showing the iteration sequence with decreasing $E_{\epsilon_{ij}}$, including (a) 2-norm residual, regularization and objective functions (7), showing the optimal iteration ($k = 8$); (b) Gaussian norms for the prior, likelihood, posterior and evidence, showing the optimal iteration ($k = 8$); (c) optimal error in predicted coefficients $\xi_{ij} - \hat{\xi}_{ij}$, with error bars from the posterior covariance (18); and (d) original and optimal predicted data and their differences.

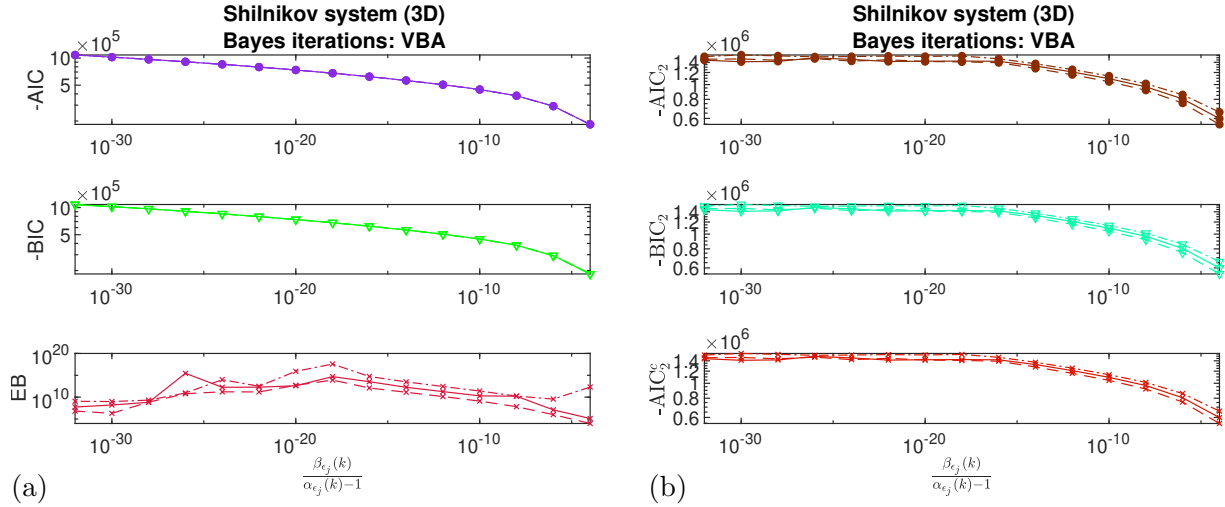


FIG. S17. Shilnikov third-order polynomial regularization using VBA, $t = 500$, $t_{step} = 0.02$, $\varepsilon = 0.02$, showing the alternative metrics by iteration sequence: (a) AIC, BIC and EB (33)-(35), and (b) 2-norm approximations to AIC, BIC and AIC_c.